Review Article | Neuroimaging and Head & Neck

http://dx.doi.org/10.3348/kjr.2014.15.5.554
pISSN 1229-6929 · eISSN 2005-8330
Korean J Radiol 2014;15(5):554-577

Korean Journal of Radiology
KJR

Perfusion Magnetic Resonance Imaging: A Comprehensive Update on Principles and Techniques

Geon-Ho Jahng, PhD[1], Ka-Loh Li, PhD[2], Leif Ostergaard, MD, PhD[3], Fernando Calamante, PhD[4]

[1]Department of Radiology, Kyung Hee University Hospital at Gangdong, College of Medicine, Kyung Hee University, Seoul 134-727, Korea; [2]Wolfson Molecular Imaging Center, The University of Manchester, Manchester M20 3LJ, UK; [3]Center for Functionally Integrative Neuroscience, Department of Neuroradiology, Aarhus University Hospital, Aarhus C 8000, Denmark; [4]Florey Institute of Neuroscience and Mental Health, Heidelberg, Victoria 3084, Australia

Perfusion is a fundamental biological function that refers to the delivery of oxygen and nutrients to tissue by means of blood flow. Perfusion MRI is sensitive to microvasculature and has been applied in a wide variety of clinical applications, including the classification of tumors, identification of stroke regions, and characterization of other diseases. Perfusion MRI techniques are classified with or without using an exogenous contrast agent. Bolus methods, with injections of a contrast agent, provide better sensitivity with higher spatial resolution, and are therefore more widely used in clinical applications. However, arterial spin-labeling methods provide a unique opportunity to measure cerebral blood flow without requiring an exogenous contrast agent and have better accuracy for quantification. Importantly, MRI-based perfusion measurements are minimally invasive overall, and do not use any radiation and radioisotopes. In this review, we describe the principles and techniques of perfusion MRI. This review summarizes comprehensive updated knowledge on the physical principles and techniques of perfusion MRI.

Index terms: *Perfusion; Perfusion MRI; Dynamic susceptibility contrast; Dynamic contrast-enhanced; Arterial spin-labeling*

INTRODUCTION

Magnetic resonance techniques have been powerful in visualizing tissue perfusion in the brain and other parts of body. Perfusion normally refers to the delivery of blood at the level of the capillaries, and measures in units of milliliters per 100 gram per minute. Perfusion is closely related to the delivery of oxygen and other nutrients to the tissue. Perfusion is, therefore, an essential parameter; and for this reason, much effort has been put into its measurement. It is important to distinguish between perfusion and bulk blood flow, which occurs along major arteries and veins.

Two main perfusion MRI approaches have been developed: those with and without the use of an exogenous contrast agent. The first group of techniques includes dynamic susceptibility contrast (DSC)-MRI and dynamic contrast-enhanced (DCE)-MRI; while the second group relates to arterial spin-labeling (ASL). DSC-MRI is used only in the brain for the clinical evaluation of perfusion in cerebral ischemia and brain tumors. This technique involves the rapid intravenous injection of a magnetic resonance contrast agent and the serial measurement of signal loss

Received May 8, 2014; accepted after revision July 5, 2014.
G.H.J. is supported by a grant of the Korean Health Technology R&D Project, Ministry for Health, Welfare & Family Affairs, Republic of Korea (A092125).

Corresponding author: Geon-Ho Jahng, PhD, Department of Radiology, Kyung Hee University Hospital at Gangdong, College of Medicine, Kyung Hee University, 892 Dongnam-ro, Gangdong-gu, Seoul 134-727, Korea.
• Tel: (822) 440-6187 • Fax: (822) 440-6932
• E-mail: ghjahng@gmail.com

Korean Journal of Radiology
KJR

during the passage of the bolus through the tissue, using T2 or T2*-weighted images. DCE-MRI is another perfusion MRI method that relies on the injection of a contrast agent, but where T1-weighted magnetic resonance images are acquired dynamically before, during, and after bolus injection of a contrast agent. The data can be interpreted in terms of physiological tissue characteristics by applying the physical principles of tracer-kinetic modeling. This method has become standard in many applications. In contrast, ASL is a perfusion MRI method for quantitatively measuring cerebral perfusion, which is also referred to as cerebral blood flow (CBF), by taking advantage of using the magnetically labeled blood itself as an endogenous tracer. ASL has been extensively performed in the research arena, and sporadically applied in diseases.

Contrast-based perfusion imaging methods require a high temporal resolution to capture the pass of the bolus, particularly when most of the contrast agent remains intravascular. These perfusion-imaging methods allow the estimation of several important hemodynamic parameters, which include blood flow, blood volume, and the mean transit time (MTT). So far, the major applications have been in the assessment and management of patients with acute stroke and tumors. Changes in hemodynamic parameters can precede abnormalities on conventional MRI, and knowledge of whether a lesion is associated with increased or decreased blood flow or blood volume can frequently help narrow the differential diagnosis and aid patient management. Additionally, measurement of contrast agent permeability, such as a transport constant related to the permeability–surface area (K^{trans}) and the fractional volume of the extravascular extracellular space (EES, v_e), may be useful to evaluate diverse diseases. Given their relationship with the underlying biology, they have been proposed as sensitive biomarkers to assess medical or surgical therapies.

The objective of this review is to describe the basic physical principles behind these techniques. The review discusses the following sections: 1) perfusion MRI methods and sources of perfusion signals, 2) physical principles of perfusion MRI, 3) perfusion MRI protocols, 4) perfusion MRI parameters, 5) perfusion signal dynamics, 6) quantifications of perfusion MRI signals, 7) sources of error, 8) current development issues, 9) outlines of clinical applications, and 10) summary of perfusion MRI. This review summarizes comprehensive updated knowledge of the physical principles and techniques of perfusion MRI.

Perfusion MRI Methods and Sources of Perfusion Signals

Table 1 lists the three major types of perfusion MRI techniques, which are the DSC-MRI, DCE-MRI, and ASL methods.

Dynamic Susceptibility Contrast (DSC)-MRI

Dynamic susceptibility contrast-MRI is one of the exogenous contrast-based methods, and relies on the intravenous injection of a paramagnetic contrast agent, such as those involving gadolinium (Gd) chelates, to generate a well-defined bolus. Most of the Gd chelates, e.g., Gd-diethylenetriaminepentacetate, are non-diffusible blood pool tracers. This technique utilizes very rapid imaging to capture the first pass of the contrast agent, and it is therefore also known as bolus tracking MRI. After the bolus of the contrast agent is injected, hemodynamic signals of DSC-MRI depend on the T_2 or T_2* relaxation time, and transiently decrease because of the increasing susceptibility effect (1).

Table 1. Three Types of Perfusion MRI Techniques

	DSC	DCE	ASL
Full term	Dynamic susceptibility contrast	Dynamic contrast enhanced	Arterial spin labeling
Bolus handling	Bolus tracking	Bolus passage	Bolus tagging
Acquisition point	First pass of contrast agent	Accumulation of contrast agent	Accumulation of tagged blood
Exogenous or endogenous	Exogenous method	Exogenous method	Endogenous method
Contrast media	Intravenous bolus injection of Gd-based contrast agent	Intravenous bolus injection of Gd-based contrast agent	Without contrast agent
Tracer	Non-diffusible blood pool tracer	Flow or permeability-limited diffusible tracer	Diffusible tracer
Relaxation mechanism	T_2/T_2* relaxation	T_1 relaxation	Magnetic labeled blood T_1 relaxation
Effect	Increased susceptibility effect	T_1 shortening effect	Blood magnetization inversion
Signal behaviors	Decreased signal	Increased signal	Subtracted signal

Dynamic Contrast-Enhanced (DCE)-MRI

Dynamic contrast-enhanced-MRI is the other exogenous contrast-based method. After the bolus of the contrast agent is injected, hemodynamic signals of DCE-MRI depend on the T_1 relaxation time, and increase because of the T_1 shortening effect associated with the paramagnetic contrast agent (2). DCE-MRI uses rapid and repeated T1-weighted images to measure the signal changes induced by the paramagnetic tracer in the tissue as a function of time. In this method, the contrast agent is also intravenously injected to generate bolus. T1-weighting is not affected by extravasation. Extracellular contrast media diffuse from the blood into the EES of tissue at a rate determined by tissue perfusion and permeability of the capillaries and their surface area. Shortening of the T_1 relaxation rate caused by the contrast medium is the mechanism of tissue enhancement (so-called T_1 or relaxivity-based methods).

Arterial Spin Labeling (ASL)

Arterial spin labeling gives absolute values of perfusion of tissue by blood. This technique utilizes arterial water as an endogenous diffusible tracer, which is usually achieved by magnetically labeling the incoming blood (3). Therefore, ASL is completely noninvasive, using no injected contrast agent or ionizing radiation and is repeatable for studying normal or abnormal physiology and its variation with time. ASL requires the subtraction of two images, one in which the incoming blood has been labeled and the other in which no labeling has occurred. The signal difference, which is the ASL signal and which removes the static tissue signal, is approximately < 1%, which makes the signal-to-noise ratio (SNR) of this method relatively low. The ASL difference signal depends on the blood T_1 relaxation time and the labeling decays after a long delay time.

Physical Principles of Perfusion MRI

Table 2 lists sources of signals of the three types of perfusion MRI techniques. The T_1 and T_2 relaxation rates (i.e., R_1 and R_2) of bulk water protons increase in the presence of paramagnetic ions and chelates, such as the gadolinium-based MRI contrast agents. This increase results from the interaction of the water protons with the unpaired electrons of the paramagnetic ion or chelate and is proportional to the concentration of the contrast agent.

DSC-MRI

This technique is based on the susceptibility changes after injecting the contrast agent. The contrast agent is a paramagnetic material, which distorts the magnetic field,

Table 2. Sources of Signals of Three Types of Perfusion MRI Techniques

	DSC	DCE	ASL
Signal contribution	Changes in T_2/T_2^* relaxation	Changes in T_1 relaxation	Magnetic blood labeling
Mechanism	Contrast agent: · Paramagnetic material · Distorts magnetic field · More susceptibility effect · Reduces T_2/T_2^* around vessel	Contrast agent: · Caused by "dipole-dipole" interactions · Interaction of protons in water molecules · T_1 reduction · Produce signal enhancement	Tagged blood by inversion · Flows into capillary sites · Exchanges into brain tissues from capillary vessel · Flows out in venous vein
Intravascular effect	Intravascular T_2/T_2^* relaxation rates (R_2/R_2^*) $R_2^* = R_{20}^* + r_2^* \cdot C_b$ $\Delta R_2^* = R_{2,post}^* - R_{2,pre}^*$	Intravascular T_1 relaxation rate R_1: $R_1 = R_{10} + r_1 \cdot C$	Intravascular T_1 blood relaxation: · Decay with T_1 of blood after tagging $R_1^{app} = R_1^{tissue} + f/\lambda$
Extravascular effect	Extravascular T_2/T_2^* relaxation: · Minor contribution of T_2 changes by slow water exchange · Tissue T_2/T_2^* changes by dephasing of extravascular spins · Decrease of T_2/T_2^* of protons in extravascular compartment	Extravascular T_1 relaxation: · Water exchange by diffusion induces T_1 change · Tracer extravasation - T_1 is shortened by short-range interactions between contrast agent particles and proton spins	Extravascular T_{1app} relaxation: · Free water exchange · Mixed with tissue water exchange · Produce apparent T_1 relaxation

Note.— ASL = arterial spin-labeling, DCE = dynamic contrast-enhanced, DSC = dynamic susceptibility contrast

Korean Journal of Radiology
KJR

and reduces T_2 around the vessel because of an increased susceptibility effect. The contrast agent increases the R_2 relaxation rate in a tissue by the relationship of (4):

$$R_2^* = R_{20}^* + r_2^* \cdot C_b \quad (1)$$

where, $R_2^* = 1/T_2^*$, R_{20}^* is the intrinsic gradient-echo transverse relaxation rate on the brain tissue without the contrast agent, r_2^* is the transverse relaxivity of the contrast agent, which depends on the blood volume and vascular morphology, and C_b is the intravascular blood concentration of the contrast agent. This relationship can also apply in a spin-echo sequence as $R_2 = R_{20} + r_2 C_b$.

Two compartments must be considered: the intravascular and extravascular compartments. When the tracer remains intravascular, the compartmentalization of the contrast agent creates strong, microscopic susceptibility gradients, which extend beyond the vessel size. The contrast agent modifies the blood T_2/T_2^* relaxation rates (R_2/R_2^*). The change of T_2/T_2^* relaxation rate (ΔR_2^*) is the subtraction of R_2^* between post- and pre-contrast injection. The T_2/T_2^* relaxation times in tissue are changed by dephasing of the extravascular spins created by the susceptibility gradients, and are thus decreased in the extravascular compartment. An approximate linear relationship exists between tissue contrast agent concentration and change in the T_2 relaxation rate, as $\Delta R_2^* = r_2^* C_b$ (5).

DCE-MRI

The relation between the DCE-MRI signal and T_1 relaxation time is dependent on the details of the MR sequence used. The contrast agent increases the R_1 relaxation rate in a tissue by the relationship of

$$R_1 = R_{10} + r_1 \cdot C \quad (2)$$

where, $R_1 = 1/T_1$, R_{10} is the intrinsic longitudinal relaxation rate of the tissue in the absence of contrast agent, r_1 is the longitudinal relaxivity of the contrast agent, and C is the concentration of the contrast agent in either blood or EES. The relaxivity is dependent upon the field strength, the chemical nature of the contrast agent and the tissue (6). The contrast concentration in tissue can be calculated if the values of r_1, T_{10}, and T_1 for the tissue are known. However, if assuming the relaxivity is independent of the tissue type (7), the outcome of the kinetic analysis of DCE-MRI data is independent of the value chosen for r_1. Recent evidence suggests that with appropriate sequence optimization, the effect of water exchange in DCE-MRI is negligible (8). Contrast agents that are rapidly extracted into the tissue are mainly monitored by T1-weighted imaging, as the resulting change is a positive increase in signal intensity, which can be clearly visualized.

ASL

This technique is based on the subtraction of an image obtained with magnetic blood labeling (known as the 'label' image) from an image obtained without labeling (known as the 'control or reference' image). Typically, for one image the water protons in the blood are tagged, such as by inverting their magnetization at the level of the large feeding arteries. Tagged blood flows into the imaging slab, following a transit delay to allow these tagged spins to enter the imaging plane and exchange with tissue. Thus, tagged blood flows into capillary sites with T_1 of blood (T_{1b}) and exchanges into tissues from capillary vessel of T_1 of tissue (T_{1t}). Some of the tagged blood can also flow out through the venous system. The resulting 'label' image reflects how, after a delay, these protons reach the capillaries in the slice of interest and diffuse in the tissue water space. The second image (the 'control' image) is obtained without labeling the incoming blood. In ideal conditions, the difference signal is proportional to the amount of blood delivered to the slice during the delay period, and therefore should reflect perfusion, since all other static effects should cancel out. In the blood vessel, the T_1 relaxation time of blood decays with the T_1 of blood after tagging. In the tissue, the T_1 of blood is exchanged almost freely and is mixed with the T_1 of tissue water. The mixed T_1 relaxation produces the apparent R_1 relaxation rate of the following equation,

$$R_1^{app} = R_1^{tissue} + f/\lambda \quad (3)$$

where f is the flow and λ is the brain-blood partition coefficient (3).

There are three broad types of labeling methods (9): pulsed ASL (PASL), continuous ASL (CASL), and velocity-selective ASL (VSASL). In CASL, the magnetization of the arterial blood flowing through a major artery is continuously labeled (usually by inversion) using radiofrequency pulses; it is based on a steady state approach (3, 10). One of the CASL labeling methods is double adiabatic inversion (11) for multi-slice acquisition. A continuous radiofrequency field

is applied for a few seconds along with a field gradient. In contrast, PASL involves a relatively short radiofrequency pulse, which results in the labeling (usually inversion) of the blood in a large region adjacent to the imaging volume. PASL labeling methods include: signal targeting with alternating radio frequency (12), flow alternating inversion recovery (13, 14), proximal inversion with control for off-resonance effects (15), transfer insensitive labeling technique (16), double inversion with proximal labeling of both tagged and control images (17), and in-plane slice-selective double inversion for both the control and the labeling scans (18). Finally, VSASL is based on a different approach and does not label the blood based on its spatial location (as in CASL and PASL), but rather does so based on its velocity (19), e.g., using binominal pulses to selectively label blood flowing below a certain velocity. This labeling is not spatially selective, avoiding transit time problems, and can be made sensitive to different blood velocities.

Perfusion MRI Protocols

Table 3 lists imaging sequences for the three types of perfusion MRI techniques.

DSC-MRI

This technique is usually based on a T2- or T2*-weighted imaging sequence, with two-dimensional (2D) or three-dimensional (3D) dynamic acquisition. Microscopic gradients cause dephasing of spins as they diffuse among these gradients, which results in signal losses in T2- and T2*-weighted images (20). When a gradient-echo (GE) acquisition is used, static field inhomogeneities are experienced in large vessels, resulting in signal losses, due to the presence of microscopic field perturbation in the vessels. In addition, dephasing in small vessels causes signal losses due to diffusion. An advantage of GE acquisitions is their increased contrast-to-noise ratio (CNR); however, a major disadvantage is their large vessel contamination. When spin-echo (SE) acquisition is used, the signal loss is greatly reduced because the dephasing is partially refocused. As with GE acquisitions, dephasing in small vessels causes signal losses due to diffusion. Therefore, SE measurements are mainly sensitive to vessel sizes comparable to the water diffusion length during the time of echo, which corresponds to capillary size vessels; whereas GE measurements are equally sensitive to all vessel sizes (4). Therefore, the SE signal theoretically yields preferential sensitivity in detecting changes in small vessels: SE-based perfusion-weighted imaging (PWI) shows a reduced appearance of large vessels and may therefore be more representative of capillary perfusion, while GE-based techniques exhibit higher CNR (21). Typically, a double dose of standard Gd chelate (0.2 mmol/kg) is injected for SE-echo planar imaging (EPI), while a single dose (0.1 mmol/

Table 3. Imaging Sequences for Three Types of Perfusion MRI Techniques

	DSC	DCE	ASL
Imaging types	T2 or T2*-weighted imaging	T1-weighted imaging	A sequence with short TE and long TR
Acquisition	2D or 3D dynamic acquisition	2D or 3D dynamic acquisition	2D or 3D single time-point or Look-Locker acquisition
Signal contributions	Large vessel: - GE: signal loss due to static inhomogenity - SE: minimizing large vessel contamination since no dephasing Small vessel: - GE and SE: dephasing and signal loss due to diffusion	Large vessels: T_1 shortening and refocusing dephasing and therefore large vessel contamination in both GE and SE Small vessel: T_1 shortening and contribution of diffusion effect The tissue concentration is sum of contribution of each subspace	Large vessel: - GE and SE: macrovascular contribution is present when no crushers or short delay times after label are used Small vessel: - GE and SE: main signal, independent on using crushers
Sequences	Common: 2D single-shot GE EPI sequence	Common: 3D GE (FSPGR, FLASH, THRIVE)	Common: single-shot GE EPI

Note.— ASL = arterial spin-labeling, DCE = dynamic contrast-enhanced, DSC = dynamic susceptibility contrast, EPI = echo planar imaging, FLASH = fast low angle shot, FSPGR = fast spoiled gradient echo, GE = gradient-echo, SE = spin-echo, TE = echo time, THRIVE = T1-weighted high resolution isotropic volume examination, TR = repetition time, 2D = two-dimensional, 3D = three-dimensional

Korean Journal of Radiology
KJR

kg) is generally injected in GE-EPI. This requires larger gauge intravenous catheters and higher injection rates (> 3 mL/s), coupled with repeated rapid cine imaging of a volume of interest, while the contrast passes through the capillary network. This acquisition requires rapid imaging sequences, such as Cartesian or spiral EPI.

DCE-MRI

This is usually scanned with a T1-weighted imaging sequence with 2D or 3D dynamic acquisition. GE measurements are sensitive to all vessel sizes, but SE measurements are more sensitive to small vessels. Commonly, 3D GE acquisition methods, such as fast spoiled gradient echo, fast low angle shot (FLASH), or T1-weighted high resolution isotropic volume examination, are used to obtain volume. For quantitative DCE-MRI, a pre-contrast mapping of T_1 is often performed. In the 3D strategy this is usually achieved by varying the flip angle (22), which runs immediately before the DCE-MRI sequence. Values of baseline T_1 for each voxel are used to calculate the post-injection T_1. In the clinical application, a constant baseline T_1 value is often used rather than mapping it because of scan time limitation. Inflow effects in the larger vessels should be minimized if arterial input function (AIF) needs to be measured. This can be done with a non-selective inversion- or saturation prepulse in a 2D acquisition.

ASL

Since the contrast for this technique is related to the preparation module (i.e., the blood labeling), ASL does not rely on the $T_2/T_2^*/T_1$ contrast of the acquisition module. It is usually scanned with a sequence with short echo time (TE) to maximize SNR and with long repetition time (TR) to allow the labeled blood to reach an imaging plane. A single time-point or dynamic acquisition using the Look-Locker method is used with 2D or 3D excitation (23-25). Commonly, a single-shot GE EPI sequence is used to obtain several slices. Furthermore, 3D-based imaging acquisition is being developed to improve the SNR (26-28).

Macrovascular signal contributions are usually dependent on two factors: a crusher gradient and a post-delay time. With a short post-delay time, the labeled blood still remains in large vessels at the time of imaging. Bipolar gradients with a very small b-value have been used to crash signals from the large vessels. Therefore, ASL signals are contributed by large vessels if crusher gradients are not used or if a short post-delay time is used after labeling; this applies for both GE and SE sequences. In contrast, this contribution can be minimized by using the crusher gradient and the long post-delay time. In this case, ASL signals are mainly contributed by small vessels. Recent developments in ASL pulse sequences were reviewed in detail in reference (29).

Perfusion MRI Parameters

Table 4 lists common imaging parameters for the three types of perfusion MRI techniques.

DSC-MRI

In DSC-MRI, a bolus of a Gd-based contrast agent administered as a short venous injection of a few seconds duration will have a width of approximately 10–15 seconds by the time it reaches the brain, creating a signal dip of about ten to twenty seconds or longer. To faithfully record the tracer concentration during this passage, images must be acquired at a rate much faster than the time it takes the bolus to pass through the tissue (i.e., MTT), which is usually of the order of several seconds. Adequate coverage of the whole brain with T2*-weighted images at a time resolution of TR < 2 seconds needs rapid imaging sequences, like EPI. TE is chosen long enough to produce sufficient CNR due to susceptibility effects, but not long enough to diphase all signals during the maximum contrast agent concentration. A

Table 4. Common Imaging Parameters for Three Types of Perfusion MRI Techniques

Imaging Parameters	DSC	DCE	ASL
TR and TE	Intermediate TR < 2 s Intermediate TE = 30–40 ms for GE	Shortest TR < 0.5 s Shortest TE < 10 ms	Long TR = 3–4 s Shortest TE = 15 ms
FA	Intermediate FA = 60–90°	Small FA = 20°	Large FA = 90°
Volume scan time	One TR	One TR*phase-encoding steps*slices	2*TR (for tagged and control scans)
Total scan duration	Relatively short (< 2 min)	Long (≈ 5 to 6 min)	Long with multiple averaging (≈ 4 min)

Note.— ASL = arterial spin-labeling, DCE = dynamic contrast-enhanced, DSC = dynamic susceptibility contrast, FA = flip angle, GE = gradient-echo, TE = echo time, TR = repetition time

relatively large flip angle is used, although not long enough to introduce unwanted T_1 contamination (30). The volume scan time is depended on TR. The scan duration is relatively short.

DCE-MRI

Dynamic contrast-enhanced MRI is scanned with very short TR and TE to generate T1-weighted images. The flip angle is also small due to short TR. The optimal setup depends to some extent on the tissue under investigation, and the clinical constraints in terms of coverage and spatial resolution, but also on the objective of the measurement. The temporal resolution of the imaging sequence is dictated by the chosen analysis technique. Thus mapping kinetic parameters from DCE-MRI traditionally requires compromise in terms of spatial resolution, temporal resolution, and volume coverage. With current MRI technique, the volume scan time is usually between 5 and 10 seconds. For the breast or other large field-of-view areas, this time is increased up to 20 seconds. The volume scan time must be as short as possible to track the contrast agent. In order to provide adequate data for pharmacokinetic analysis data, collection will typically continue for in excess of 5 minutes. The length of the total acquisition time is particularly important for accurate measurement of the fractional volume of EES, v_e.

Recently, a new dual temporal resolution-based, high spatial resolution, pharmacokinetic parametric mapping method has been described (31). In the protocol, a high temporal resolution pre-bolus is followed by a high spatial resolution main bolus to allow high spatial resolution parametric mapping for tumors. The measured plasma concentration curves from the dual-bolus data were used to reconstruct the high temporal resolution AIF necessary for accurate kinetic analysis. The high temporal resolution (sampling interval = 1 second) pre-bolus data can also be used for tissue perfusion mapping.

ASL

Arterial spin labeling is scanned with a relatively long TR to allow for the labeled blood to travel and exchange with the tissue and short TE to maximize SNR. The arrival time of the labeled blood into the imaging slices is even longer in CASL than in PASL. Since the long labeling duration and the long arterial transit time are longer in CASL, TR in CASL is usually longer than that in PASL. The exchange time from the intravascular to extravascular space is about 1 second for both CASL and PASL. Because of the long TR, a large flip angle is also used. The ASL volume scan time is dependent on 2 x TR because two images (the label and control images) must be acquired for each volume. The scan duration is also relatively long because of the need for multiple repeated scans to increase SNR. It is not uncommon to acquire at least 40 averages to improve SNR. A group consensus recommendation for a protocol for clinical applications was recently published in reference (32).

Perfusion Signal Dynamics

DSC-MRI

The model used for perfusion quantification is based on the physical principles of tracer kinetics for non-diffusable tracers (33) and relies on the assumption that the contrast material remains intravascular in the presence of an intact brain-blood barrier (BBB). The DSC-MRI signal intensity time course (in arbitrary units) for a voxel represents the hemodynamics of the contrast agent (Fig. 1). Series images are acquired before, during, and after injecting the contrast agent. While passing through the microvasculature, a bolus of the contrast agent produces decreases in the MR signal intensity. The time course images can be divided into three stages: the baseline, the first passage of the bolus, and the recirculation period (34). During the baseline period, images are acquired before the arrival of the bolus, and the time course signals are therefore usually constant. During the first passage of the contrast agent, the contrast

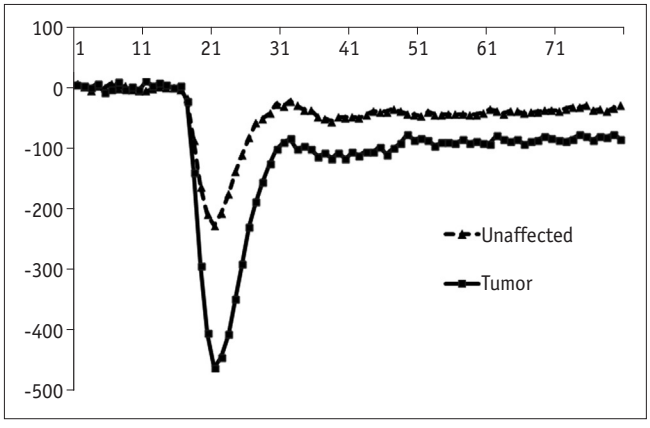

Fig. 1. Hemodynamics of contrast agent obtained with dynamic susceptibility contrast MRI signal intensity time course (in arbitrary units), for voxel. Series images are acquired before, during, and after injecting contrast agent. While passing through microvasculature, bolus of contrast agent produces decreases in magnetic resonance signal intensity.

Korean Journal of Radiology
KJR

agent arrives at the voxel and the DSC-MRI signal quickly decreases until the peak signal change (corresponding to the time of maximum contrast agent concentration). After the minimum signal is reached, the signal intensity (partially) returns to baseline values. Finally, during the recirculation period (which often partially overlaps with the first passage), the DSC-MRI signal decreases again (although to a smaller degree and a slower rate), due to re-entering the contrast agent. After this period, signals theoretically recover up to the baseline. The signal intensity-versus-time curves are converted into concentration-versus-time curves, assuming a linear relationship between the change in relaxation rate, and the concentration. A gamma-variate function (35) is then sometimes fitted to the resulting concentration time course, to eliminate the contribution of tracer recirculation.

DCE-MRI

The time course of enhancement is related to the changes, which depend on the physiological parameters of the microvasculature in the lesion and on the volume fractions of the various tissue compartments. Three major factors determine the behavior of low-molecular-weight contrast medium in tissues during the first few minutes after injection: blood perfusion, transport of contrast agent across vessel walls, and diffusion of contrast medium in the interstitial space. Overall, for a bolus injection of the contrast agent into the blood circulation, there is always an initial increase in its concentration in the plasma and possibly some leakage into the interstitium for the duration of the injection (Fig. 2). Afterwards, the plasma concentration continuously decreases because of diffusion into the body and clearance through the kidneys to the urine; whereas the tissue concentration can increase for a while and then decrease, depending on various physiological variables. The dynamic acquisition pattern is similar to that of DSC-MRI: images are acquired before, during, and after injecting the contrast agent. Most benign and malignant lesions show signal enhancement in the first few minutes after bolus administration of a Gd-based contrast agent. The normal tissue may also show enhancement.

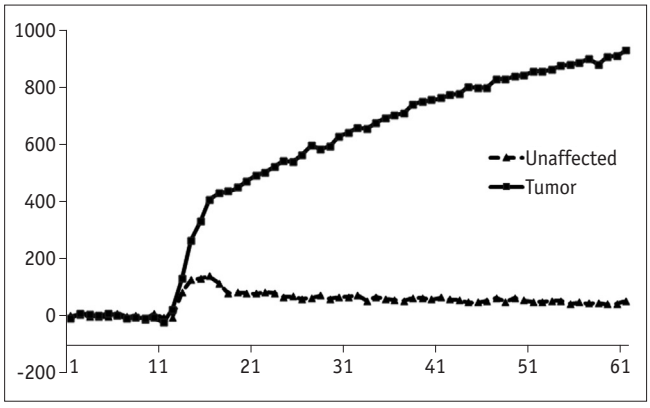

Fig. 2. Hemodynamics of contrast agent obtained with dynamic contrast-enhanced MRI signal intensity time course (in arbitrary units), for voxel. Time course of enhancement is depended on physiological parameters of microvasculature in lesion, and on volume fractions of various tissue compartments. For bolus injection of contrast agent into blood circulation, there is always initial increase in its concentration in plasma.

ASL

In routine PASL and CASL approaches, the signal at a single inversion time or post-labeling delay of around 1.5–1.8 seconds is often used in clinical studies; this single-time point approach can approximately calculate blood flow (32) without having information about the arterial transit time. To minimize the definition error of the bolus width of labeled blood in a single-time point experiment on PASL, two labeling times were introduced in a sequence known as quantitative imaging of perfusion using a single subtraction (QUIPSS II) (36). In this sequence, the first labeling time (TI1) was defined by the interval between the labeling pulse and a saturation pulse, which effectively defined the labeled bolus width. The second labeling time (TI2) was defined by the interval between the labeling pulse and the excitation pulse of image acquisitions. This method can be used with any labeling techniques and is involved by the saturation of the inverted region a short time after inversion. This saturation acts to chop off the tail of the bolus, reducing the arrival time sensitivity. This method can be used to minimize quantification errors of blood flow with a long TI2 labeling time for PASL during data acquisition (36, 37). A similar strategy was also proposed for CASL to minimize the arterial transit time error in the single measurement, which is based on a long post-labeling delay (PLD) time of typically 0.9–1.5 seconds between the tagging and the readout (38, 39); this PLD must be longer than the longest transit time. For the single-time point ASL, a single compartment model is used for flow quantification with the concept of free diffusible water and, despite their simplifying assumptions, they are recommended for most clinical studies (32).

Alternatively, ASL signals can be acquired with increasing labeling times or delay times. Figure 3 shows the subtracted hemodynamic signal between control and labeled images on

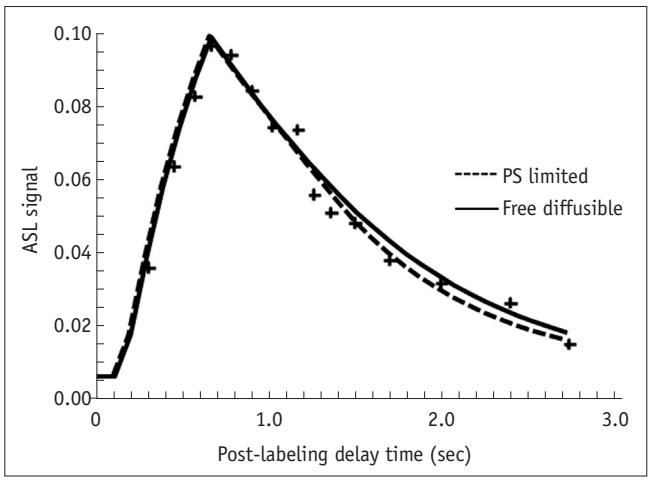

Fig. 3. Subtracted hemodynamic signal between control and labeled images on arterial spin labeling (ASL) experiment.
Curve shows three phases, which are baseline period, arterial transit and exchange period of labeled protons, and decayed period of labeled protons. PS = permeability surface area product

an ASL experiment. The curve shows three phases. The first phase is the baseline period. The ASL signal in this phase is zero since the labeled protons have yet to reach the tissue voxel in the slice. The second phase is the arterial transit and the exchanging period of the labeled protons. The ASL signal in this phase increases as the labeled protons enter the voxel and exchange from intravascular to extravasular tissues. The signal peaks at around 1 second delay time. Protons in blood diffuse from intravascular space to extracellular space with a certain exchanging time. At higher flow rates, the exchange appears restricted (40), as though the water channels have been saturated. The third phase is the decayed period of the labeled protons. The ASL signal decreases as labeled protons leave the tissue voxel and decay due to the longitudinal T_1 relaxation time. This whole dynamic scan acquired with multi-time point data has the benefit of also providing measures of arterial transit time (ATT) of the tagged blood in the voxel and the exchanging rate (T_{ex}) in addition to the blood volume and flow (41).

Quantifications of Perfusion MRI Signals

Table 5 lists quantifications of the three types of perfusion MRI signals.

DSC-MRI

In DSC-MRI data, original model assumptions are intact BBB, stable flow during the measurement, and negligible T_1 changes after injecting the contrast media. Additional assumptions are no recirculation of the tracer, which can be removed by fitting to a gamma-variate function, and no dispersion or delay of the bolus for estimating the AIF. The physical principles of the indicator dilution theory are based on the central volume principle which is that cerebral blood flow equals cerebral blood volume divided by mean transit time (42). The convolution theory was used to evaluate the concentration of the hemodynamic changes of the contrast agent (34):

$$C(t) = CBF \cdot AIF(t) \otimes R(t) \qquad (4)$$

Furthermore, a leakage correction technique was used to consider the effect of leakage of the contrast agent from the vessel to tissue, such as the method to correct for leakage in cerebral blood volume (CBV) quantification (43).

Quantitative parameters, often referred to as 'summary parameters' (44), can be obtained without considering a physiological basis, or using deconvolution and an AIF. Those parameters are time-to-peak (TTP), T0 (bolus arrival time), full width at half maximum, the first moment of the peak (FM or $C^{(1)}$), and maximum peak concentration. Alternatively, quantitative hemodynamic indices with physiological basis can be derived by measuring an AIF a deconvolution analysis, such as CBF, CBV, MTT, and the permeability.

In particular, CBV can be determined from the ratio of the areas under the tissue and arterial concentration time curves, respectively (45). In general, relative CBV values are reported because of the complexities in measuring an absolute AIF (46). Assuming uniform arterial concentration areas in all arterial inputs, relative CBV measurements are determined by simply integrating the area under the concentration time curve (47), and by applying a gamma variate function (48) or an independent component analysis (49) to correct for tracer recirculation. CBV is proportional to the area under the peak and its measurement can be insensitive to bolus delay and dispersion.

To obtain CBF, the feeding artery of tissue element and the tissue retention of tracer must be calculated. The first term is termed the AIF and the second term is termed the residue function, R. The concentration of contrast agent present in the tissue at a given time is the multiplication of a constant, which is termed the CBF, and the amount of blood with tracer concentration AIF passing through the tissue element per unit time. The residue function R

Korean Journal of Radiology
KJR

Table 5. Quantifications of Three Types of Perfusion MRI Signals

	DSC	DCE	ASL
Model assumptions and considerations	Original model assumptions: · Intact BBB · Stable flow during the measurement · Negligible T_1 change	Model considerations: · Known T_1 maps before injection of Gd to calculate Gd concentration · Instantaneously and well mixed contrast agent	Model considerations: · Inversion efficiency (α = 0–1) · Blood (T_{1b}) and tissue (T_{1t}) T_1 · Inflow and outflow effects · Blood-tissue partition coefficient of water (λ)
Additional assumptions and considerations	Additional assumption: · No recirculation of tracer · No dispersion and delay of bolus for estimating AIF	CBF under conditions of: · High PS (i.e., flow-limited) · Blood plasma volume (v_p) not too big (IV tracer not modeled well)	Additional considerations: · Arterial transit time · Vascular signal contamination
Theoretical modeling	Dilution theory: · Central volume principle (CBF = CBV/MTT) · Gamma-variate function to remove recirculation Convolution: · C(t) = CBF (AIF(t) $\otimes$ R(t)) · Leakage correction for CBV	Flow-limited or high permeability model for small MW agents: · K^{trans} = EF = F where E $\approx$ 1 Mixed condition: · K^{trans} = E*F = (extraction * flow) where E = (1 - exp [-PS/F]) PS limited model or low permeability model for MW > 50 kD agents: · K^{trans} = E*F = PS where E = PS/F	Single TI quantification: · Instantaneous or fast exchange · Single compartment model with uniform plug flow · PWI is directly related to CBF · Developed a general kinetic model or Buxton model Dynamic ASL quantification: · Multiple TI or PLD times · Hemodynamic model
Quantitative parameters	Quantitative, but no physiological basis: · TTP · BAT or T0 · FWHM · First moment of peak · MPC	Quantitative, but no physiological basis: · AUC · Initial AUC (uptake part only) · T0 · TTP · Maximum signal difference · Uptake rate (maximum slope)	Single TI quantification: · Calculate CBF only Dynamic ASL quantification: · T0, TTP, and Tex
Physiological quantitative parameters	Quantitative, with physiological basis: · Absolute CBF · Relative CBF · CBV, MTT · Permeability	Quantitative, with physiological basis: · K^{trans} · k_{ep} · v_e · v_p	Quantitative, with physiological basis: · Absolute CBF

Note.— AIF = arterial input function, ASL = arterial spin-labeling, AUC = area under curve, BAT = bolus arrival time or T0, BBB = brain-blood barrier, CBF = cerebral blood flow, CBV = cerebral blood volume, DCE = dynamic contrast-enhanced, DSC = dynamic susceptibility contrast, E = extraction, F = flow, FWHM = full width at half maximum, Gd = gadolinium, MPC = maximum peak concentration, MTT = mean transit time, MW = molecular weight, PLD = post-labeling delay, PS = permeability surface area product, PWI = perfusion-weighted imaging, Tex = exchanging time, TTP = time-to-peak

describes the probability that a molecule of tracer that entered a voxel at t = 0, following an ideal instantaneous input, is still inside that voxel at a later time t. It depends on the transport of the tracer between blood and tissue and the subsequent clearance from the tissue volume. The tissue concentration time curve becomes the convolution of the tissue impulse response function and the shape of the AIF. The product CBF*R is termed the tissue impulse response function, which is the tissue concentration as a result of the aforementioned impulse input. With known AIF, the tissue impulse response function has to be determined by deconvolution, essentially estimating CBF*R from the experimental data. Finally, CBF is determined as the initial height of the tissue impulse response function at t = 0 (note: due to the presence of bolus dispersion and other possible deconvolution related errors, CBF is most commonly estimated from the maximum value of the impulse response, rather than from its initial value (50)). The most commonly

used approaches to perform the deconvolution are based on a model-independent method, in which no functional shape assumptions are made regarding the residue function; these include singular value decomposition (SVD) (34, 51-53) and its delay-insensitive variant circular SVD (53), Fourier-based methods (54), Tikhonov-based methods (55, 56), iterative methods (57-60), and Bayesian methods (61-63). To obtain CBF, values for the density of tissue, large-vessel hematocrit values, and a uniform value for the capillary hematocrit are often assumed. AIF in practice is estimated from a major artery, such as the middle cerebral artery or the internal carotid artery with the assumption that this represents the exact input to the tissue.

The calculation of MTT requires knowledge of the transport function or CBF, by the central volume theorem, which is MTT = CBV/CBF. A further common parameter in clinical studies that can be obtained after deconvolution is the so-called T_{max} parameter: the TTP of the impulse response function (64). This parameter has been shown to primarily be a measure of macrovascular status (65).

DCE-MRI

Signal enhancement seen on a dynamic acquisition of T1-weighted images can be assessed in two ways: by the analysis of signal intensity changes (semi-quantitative) or by quantifying contrast medium concentration change using a pharmacokinetic modeling technique. Semi-quantitative parameters describe tissue signal intensity enhancement using a number of descriptors (66). These parameters without considering physiological basis include area under curve (AUC), initial AUC (uptake part only), initial time (T0), TTP, maximum signal difference, uptake rate (maximum slope), and signal enhancement ratio. A recent publication (67) compared semi-quantitative and pharmacokinetic parameters for the analysis of DCE-MRI data and investigated error-propagation in semi-quantitative parameters.

Quantitative hemodynamic indices can be derived with physiological basis. Most methods have used a compartmental analysis to obtain some physiological parameters: the transfer constant (K^{trans}), the rate constant or reflux rate ($k_{ep} = K^{trans}/v_e$), the EES fractional volume (v_e), and fractional plasma volume (v_p). The transfer constant K^{trans} has several physiologic interpretations, depending on the balance between capillary permeability and blood flow in the tissue of interest. The rate constant k_{ep} is formally the reflux rate constant between the EES and blood plasma. Both the transfer constant and the rate constant have the same units (1/minute). The rate constant k_{ep} is always greater than the transfer constant K^{trans} (because $v_e < 1$). The general equation to express the hemodynamic event after injecting the contrast agent is:

$$C_t(t) = v_pC_p(t) + K^{trans} \int_0^t C_p(\tau) \exp\left(-\frac{K^{trans}}{v_e}[t-\tau]\right)d\tau \quad (5)$$

This is often referred to as the extended Tofts model (68). In the extended Tofts model, K^{trans} is interpreted differently under flow-limited and permeability-limited conditions. If the delivery of the contrast medium to a tissue is insufficient (flow-limited situations or where vascular permeability is greater than inflow), then blood perfusion will be the dominant factor that determines contrast agent kinetics and the transfer constant, K^{trans}, approximates to tissue blood flow per unit volume (66). If tissue perfusion is sufficient, and transport out of the vasculature does not deplete intravascular contrast medium concentration (non-flow-limited situations), then transport across the vessel wall is the major factor that determines the contrast medium kinetics (K^{trans} then approximates to the permeability surface area product). A computer simulation work has demonstrated that using a sampling interval shorter than half the duration of the first pass of AIF will be essential in kinetic analysis using the extended Tofts model (31). A temporal resolution of around 5 seconds is typically used in these studies. Efforts have been made on developing models that enable separate estimates of perfusion and capillary permeability, rather than a single parameter K^{trans} that represents a combination of the two. A variety of such models have been proposed in the literature (69-71). However, these models demand both high temporal resolution (typically 1 second), and good SNR in the data and have therefore not been widely employed.

ASL

In ASL data, a quantification model should consider the inversion efficiency (α = 0–1), blood (T_{1b}) and tissue (T_{1t}) T_1 relaxation time, inflow and outflow effects, and blood-tissue partition coefficient of water (λ), ATT (δ), and vascular signal contamination. The subtracted images from control to label are PWI. The relationship between the PWI signal and the actual CBF depends mainly on the proton density and T_1 relaxation rates of tissue and inflowing blood, and their respective differences. In addition, the ATT from the inversion slab to the observed region in the

Korean Journal of Radiology
KJR

images is also an important factor.

A simple way to obtain the quantitative blood flow is carried out using the tracer clearance theory originally proposed by Kety and Schmidt (72), which was first adapted to ASL experiments by Detre et al. (3) and Williams et al. (10). In single labeling delaying time (TI) quantification, it is assumed that the tagged arterial blood water is a free diffusible tracer, implying that the exchange of blood water with tissue water happens instantaneously upon its arrival at the parenchyma. Therefore, this model corresponds to a single compartment tracer kinetic, described by a mono-exponential tissue response function. A general kinetic model for analyzing the difference in longitudinal magnetization in the tissue due to labeled blood (73) is:

$$\Delta M = 2 \cdot M_{0a} f \int_0^t c(\tau) \cdot r(t-\tau) \cdot m(t-\tau) d\tau \qquad (6)$$

where, M_{0a} is the equilibrium magnetization in a blood filled arterial voxel, and c(t) is the delivery function or AIF similar to DSC and DCE-MRI. The residue function r(t-τ) describes the washout of tagged spins from a voxel, and m(t-τ) includes the longitudinal magnetization relaxation effects. The magnetization difference due to tagging is proportional to the equilibrium magnetization of the blood and to blood flow. For the quantification of dynamic ASL MRI data, a hemodynamic model can be used for the multiple TI times for PASL or the multiple PLD times for CASL. In this case, in addition to blood flow (BF), the arrival time (T0) of tagged blood in the voxel, TTP, and the exchanging time (T_{ex}) from the intravascular to extravascular space can be obtained (41).

Sources of Error

DSC-MRI

A number of sources of error can affect CBF quantification using DSC-MRI (74). The major sources of error include:

Linear Relationship between Magnetic Resonance Signals and the Concentration of the Contrast Agent

One of the fundamental assumptions in the magnetic resonance tracer model is that the relaxation rate is linearly proportional to the intravascular concentration of the contrast agent (20). However, the relaxation rate measured inside arteries will vary nonlinearly and thus the linear assumption can introduce systematic errors for absolute quantification (75).

Delay of the Bolus for Estimating Arterial Input Function

Depending on the choice of deconvolution algorithm, bolus delay can introduce an underestimation of the calculated flow and overestimation of the MTT with carotid stenosis or occlusion (52); this is particularly the case for the standard SVD method (34, 51, 52), and modifications have been proposed to make it delay-insensitive (53).

Dispersion of the Bolus

In patients with vascular abnormalities (e.g., stenosis or occlusion), it is possible for the bolus not only to get delayed in its transit to the tissue, but also to get spread in time (i.e., dispersed) (76, 77). This effect has been shown to lead to CBF underestimation and MTT overestimation (52). One way to minimize this source of error is by measuring a local AIF, closer to the tissue of interest (78-80).

Partial Volume Effect

The measurement of AIF is also associated with partial volume effects as a result of the relatively low spatial resolution of the images commonly used in DSC-MRI (81). Interestingly, it has recently been shown that despite the presence of partial volume, a good estimate of the shape of the AIF can be obtained by measuring the signal changes in specific location near (but completely outside) the middle cerebral artery (82, 83).

Leakage Correction

The presence of a BBB breakdown results in leakage of the tracer into the extravascular space. In this situation, tissues have the direct strong relaxation effects that the T_1 and T_2* of the tissue are decreased. This leads to systematic errors in the DSC signal change. To minimize this effect, more sophisticated models of the first pass kinetics should be applied (84).

Uniform Tissue r_2 Relaxivity

The relaxivity between the MR signal and the contrast agent concentration is assumed to be uniform across different tissues. Tissue with different proportions of blood vessels could have different relaxivities (20, 85). The relaxivity of the extravascular tissue signal could depend on the pulse sequence parameters. However, any systematic errors in the assumption of r_2 relaxivity will be canceled in the calculation of the MTT because of the ratio of CBV and BF.

Absolute Units

In order to quantify CBF in absolute units (i.e., milliliters per 100 gram per minute) it is important that a patient-specific scaling factor is used. Several such methods have now been proposed, including those based on complementary CBV measurements (86), ASL measurements (87), and phase contrast MR angiographic measurements (88).

DCE-MRI

Imaging Artifacts

Echo planar imaging is not good for DCE-MRI, since it has a high susceptibility-related artifact. Snapshot FLASH is also not good because of suffering from point-spread function problems (89). Motion artifacts generally cause a degradation in image quality.

Temporal and Spatial Resolutions

A model requires high temporal resolution to provide a comprehensive description of the underlying causes of contrast agent uptake in a tissue. With a low temporal resolution, inaccurate AIF may be obtained. With low spatial resolution, a partial volume effect may also cause inaccurate measurements of AIF.

Kinetic Modeling

First, the use of less detailed or less accurate models may introduce systematic errors into the kinetic parameters being evaluated. For example, non-inclusion of a vascular volume v_p can lead to significant errors in the fitted values of K^{trans} (90). Second, a value for the *in vivo* relaxivity of the contrast agent has to be assumed to calculate the concentration of the contrast agent based on the value obtained from *in vitro* measurements. However, the relaxivity value depends on tissue types and water compartments (6), leading to errors in concentration values. Third, the measurement of contrast agent concentration may be inaccurate during the determination of kinetic parameters when water exchange between the compartments is not accurately considered (91). Fourth, kinetic parameters may have errors if the plasma transit time is not considered in the kinetic model. Finally, most of the significant source of error is related to the T_1 values used. In clinical applications, an additional scan to measure T_1 is not performed because of time limitation. Although people try to scan T_1 measurement, a rapid acquisition technique, such as a two-point method, is often used, which causes unreliable measurement of T_1 values in tissues. This can cause inaccurate estimation of kinetic parameters.

ASL

Labeling Efficiency

An error in the labeling efficiency produces large errors in the perfusion estimation. In order to include all signals from perfusing blood, they must be efficiently labeled. It is not practical to measure the labeling efficiency for every subject, so this will cause some error to the measurement. For the CASL technique, the labeling efficiency is about 70% for multi-slice imaging (11), owing to the added inefficiency of the amplitude modulated control. For the PASL techniques, the labeling slab can only extend as far as the head coil, and a gap must be present between the image slice and the labeling slab to avoid errors due to imperfect slice profiles of the labeling pulses. To improve the labeling efficiency, better labeling pulses have been developed, such as the hyperbolic scant pulse (92), frequency offset corrected inversion pulse (93), and bandwidth-modulated adiabatic selective saturation and inversion pulse (94).

Contribution of Static Tissue Signals

During the subtraction between control and labeled images, a perfect canceling-out of static tissues is usually assumed. However, this tissue contribution in the subtracted signals degrades PWI contrast. To minimize these static tissue signals, background suppression techniques were developed (95, 96). Since background suppression does reduce ASL signals, there is still debate as to whether or how much background suppression to use (97). Furthermore, the labeling pulse can cause substantial magnetization transfer (MT) effects in the static tissue of the image slices, particularly with CASL, due to the long labeling. The control image has the same MT effects as the labeling image, so that they will cancel on subtraction.

Quantification Model Errors

The ASL signal is dependent on several factors: the inversion efficiency, blood T_1, tissue T_1, capillary permeability, arrival time, and perfusion. These factors can be sources of error in the quantification of ASL signals if we do not take them into account in the model. These factors can either be assumed or measured. The first factor is the blood T_1 value. An accurate measurement of blood T_1 is difficult due to the movement of the blood. Most models

Korean Journal of Radiology
KJR

use a constant value, which will be a source of error in perfusion quantification. In addition, tissue T_1 should be measured to eliminate errors in perfusion quantification. However, T_1 measurement in tissue can usually take a relatively long time, thus extending the total acquisition time. A fast mapping technique was proposed to map tissue T_1 within a few seconds (98). The further source of error for perfusion quantification is the assumption of the free diffusion of water in a well-mixed tissue compartment (3, 13). More complex models, such as a two-compartment model with separate blood and tissue components, are recommended to reduce the error (39). Neglect of the arrival time or capillary permeability can lead to large errors in perfusion quantification.

Arterial Transit Time

Arterial transit time is one of the major sources of errors in the quantitative estimate of cerebral perfusion. This value differs across the brain even in healthy subjects, being longest in distal branches, especially in the regions between perfusion territories also known as border-zone areas. Most clinical applications of ASL are used with a single time-point scan to minimize the total scan time. In this situation, the CBF value in each voxel is under- or over-estimated due to varying ATT from the labeling region to the imaged tissue in each voxel. Previous functional MRI studies showed that ATT varies between baseline and activation conditions (99, 100). Several techniques were proposed to minimize transit time errors in the measurements of perfusion (36, 39). These include the QUIPSS II technique with a single time-point measurement on PASL (36). For CASL, an increase in the delay time before imaging reduces arrival time sensitivity on the single time-point measurement (39). Measurement of transit time typically requires the acquisition of multiple images with different delay time in CASL or different labeling time in PASL (23, 100, 101). However, this causes an extension of scan time. Mapping of ATT can help to improve CBF quantification and may also provide additional information of a vascular condition.

Partial Volume Errors

Arterial spin-labeling is most often acquired with relative low spatial resolution and, therefore, partial volume effects can be substantial. This can lead to significant quantification errors, for example, in patients with atrophy. To minimize this source of error, partial volume correction methods have been proposed for single time-point ASL protocols (102, 103) and multi-delay protocols (104).

Current Development Issues

DSC-MRI

For DSC-MRI, the AIF is obtained from a major large supplying artery. To improve the detection of AIF, local AIF near the lesion or voxel of interest could be used (78-80). However, in this case, the partial volume effect could be a source of error. Therefore, a method should be developed to minimize the partial volume effect.

To improve the quantification of data, nonlinear behaviors between $\Delta R2^*$ and the contrast agent should be taken into account (75, 81, 105). In addition, corrections of hematocrit amount for each subject and dispersion need to be considered (61). To minimize the bolus dispersion, a local small vessel close to the tissue voxel rather than a global large vessel can be used to detect AIF; however, further work is needed to validate such local AIF approaches. There is also much interest and potential in the use of phase information to obtain AIF estimates (106).

Finally, there has been increasing interest in developing fully automatic methods, with embedding more sophisticated mathematical approaches to take account of susceptibility-induced relaxation alternations in tissue, AIF automatic searching methods, robust deconvolution algorithms, etc. (107-109). These automatic methods should facilitate the widespread use of advanced DSC-MRI analysis methods, as well as improve reproducibility, and offer faster analysis.

DCE-MRI

For DCE-MRI, the quantification model should be improved, to consider the incomplete exchange of intravascular and extravascular water. This is termed a tissue homogeneity model. In addition, plasma transit time or plasma MTT needs to be considered. There is a tradeoff between the temporal resolution and spatial resolution. The imaging protocol has to improve to increase both resolutions, for example, using the compressed sensing (CS) technique. Measurement of AIF in DCE-MRI was performed as that in DSC-MRI. The effects of variable proton exchange rates need to be incorporated into a kinetic model. To increase acquisition speed to improve the detection of AIF, it can be of benefit to apply a new acquisition and reconstruction method, such as a CS technique.

Pseudo CASL (PCASL)

Recently, PCASL was introduced, to address some of the weaknesses of the CASL approach (110). PCASL uses a long series of short radiofrequency and gradient pulses to replace the continuous pulse in CASL. PCASL optimizes pulse trains to adapt to pulsatile flow, reduces sensitivity to off-resonance conditions, and reduces specific absorption rate. Advantages of PCASL over CASL are improvement of the magnetization transfer effect, and ease of implementation on clinical imaging systems for radiofrequency and gradients without using any special additional hardware. Currently, the PCASL tagging method provides the best SNR. However, one of PCASL's possible problems is its increased sensitivity to off-resonance effects, which lead to reduced labeling efficiency. Various methods are currently available to minimize this effect (29).

Minimization of Static Tissue Contribution

For ASL MRI, SNR can be improved by minimizing static tissue contributions with saturation of static tissue signals. It is beneficial to reduce the signal from static tissue to improve SNR and reduce physiological sources, such as cardiac, respiratory, and subject motion. Currently, multiple inversion recovery pulses known as background suppression are applied to minimize tissue signals, in the subtraction of control and tagged images (95, 96, 111). For sequential acquisition of the multi-slice images, background suppression has different levels of effectiveness across slices, as each slice is acquired at a different point in time. This is most effective for 3D imaging methods, where there is only one excitation following each label.

Vascular Territory Mapping

In addition to providing quantitative measures of CBF, ASL methods have recently been developed to provide anatomic delineation of the vascular territories of feeding arteries, such as the internal carotid arteries and the vertebral arteries in the brain. The selective ASL methods can be used to visualize the individual territories of brain-feeding and cerebral arteries, rather than to provide nonselective cerebral perfusion maps. Vascular territory imaging techniques for perfusion imaging are currently employed in CASL (112-114), PASL (115-118), and PCASL (119-121). Detailed reviews of the perfusion territory mapping using ASL are found in the literature (29, 122). These methods are potentially useful for risk assessment, and treatment planning and monitoring in cerebrovascular disease, as well as in the identification of blood supplies to tumors and arteriovenous malformations.

Multiband Radiofrequency Excitation

General ASL scan methods have a limitation on the number of image slices for spatial coverage possible within the time between delivery of labeled water to capillaries with exchange into the brain parenchymal and T_1 decay. This limitation can be overcome in pulse sequence design to allow simultaneous multi-slice scans, with a method known as multiband excitation (123). This is a parallel imaging technique that simultaneously excites multiple slices with a multiband excitation pulse and reads out these images in an echo train. This technique was incorporated in ASL with the aim of increasing spatial coverage without lengthening the time window of image readout within the capillary phase of blood circulation (124, 125). The application of this technique can be extended to any ASL variant, such as PASL, CASL, and PCASL.

Beyond CBF Measurements

Arterial spin-labeling can provide information on the vascular supply to tissue and is developed to map several physiological parameters, in addition to CBF. ASL methods can be used to obtain angiography (126, 127), to quantify the blood volume of the arterioles and capillaries prior to the diffusion of the tracer out of the microvasculature (24, 128), and to assess vascular permeability to water, and characterize the BBB (41, 129).

Outlines of Clinical Applications

This is a methodological and technological review of perfusion MRI methods and, therefore, we do not intend to thoroughly cover the clinical applications. However, we include this brief section to illustrate some of their clinical applications. The technical, physical, and contrast-related properties of the methods affect how they can be and are used clinically. For example, for stroke, neurons die at a rate of 2 million per minute (130), and the success of thrombolytic therapy is critically dependent on minimizing the 'door-to-needle' time. Therefore, minutes matter in the diagnostic imaging of patients. This is a challenge for ASL because of its longer protocols–and even DSC-MRI is under increasing pressure, because some clinicians save

Korean Journal of Radiology
KJR

time by just acquiring diffusion-weighted imaging. So we must develop and prove the clinical utility of perfusion MRI methods in a clinical setting. For cerebrovascular diseases (carotid stenosis, etc.), it is crucial to quantify the change in CBF to a standardized vasodilator signal to ascertain whether the patient has exhausted cerebrovascular reserve capacity, and needs surgery. Due to some of the issues associated with quantifying DSC-MRI in absolute units and the need for repeated measurement to measure the CBF change, ASL might be preferable for this application. In Alzheimer's disease, CBF is not a diagnostic criterion, but progression of hypoperfusion over time may be an important tool for the evaluation of therapeutic interventions. Again, quantitative CBF is crucial for this, so ASL might be preferable. Finally, a related issue that must be taken into consideration is that of availability: for many hospitals, DSC-MRI is easier to perform than ASL, which is a likely reason for the limited work carried out so far to prove ASL's clinical utility. The recently published ASL consensus paper with recommendations for its implementation for clinical applications is expected to make a big step towards addressing this issue. Table 6 lists some of the most common clinical applications of the three types of perfusion MRI methods.

DSC-MRI

Dynamic susceptibility contrast-MRI remains the standard for perfusion MRI of the brain (131, 132), but several studies have shown that DCE-MRI is a viable alternative (133-137). DSC-MRI is only applied in brain diseases, such as stroke and tumors. Permeability imaging with DSC-MRI has been proposed (138-141), but DCE-MRI remains the method of choice for this purpose (131, 142, 143). Clinical applications of DSC-MRI continue to evolve in the diagnosis and management of brain diseases, including acute stoke, intracranial neoplasms, and dementia. Figure 4 shows MR images (A) and parameter maps calculated from DSC-MRI (B) and DCE-MRI (C) data obtained from a patient who has anaplastic astrocytoma (World Health Organization grade III) in the frontal lobe in the brain. Figure 4A shows the T2-weighted image, fluid attenuated inversion recovery image (FLAIR), and T1-weighted images before (Pre-T1WI), and after (CE T1WI) contrast enhancement. The lesion has high signal intensity on both the T2-weighted and FLAIR images, but has low intensity on both T1-weighted images. The lack of signal enhancement on contrast-enhanced T1WI indicates that the BBB in the lesion is intact. Figure 4B shows the parameter maps calculated from DSC-MRI data obtained from the patient shown in Figure 4A. Increased CBV, CBF, and leakage (K2) values are shown in the frontal lesion, indicating that tumor vascularity is increased.

DCE-MRI

Dynamic contrast-enhanced-MRI is also often applied in brain diseases, especially tumors. Nowadays, this method is routinely applied in patients with breast, prostate, pelvic, and muscle diseases. This method is popular in assessing drug therapy. DCE-MRI is the standard approach for perfusion imaging outside the brain (144-150). DCE-MRI is useful in accurately mapping blood volumes in a tumor lesion in addition to K^{trans}. This technique can be used in investigations of tumor grades, the treatment effect of radiotherapy, or the monitoring of treatment response to chemotherapy. Figure 4C shows the parameter maps

Table 6. Common Clinical Applications of Three Types of Perfusion MRI Signals

	DSC	DCE	ASL
Brain	Brain (most) Stroke Tumor	Brain (less) Tumor	Brain (some)
Other than brain		Breast Prostate Pelvic Muscle	Heart Kidney Muscle
Good indications	Popular to define ischemic penumbra in stroke	Popular in assessing drug therapy	Attractive for poor IV access, infants and children, pregnant women, functional MRI including functional connectivity and connectome applications, vascular reactivity studies, and vessel selective labeling

Note.— ASL = arterial spin-labeling, DCE = dynamic contrast-enhanced, DSC = dynamic susceptibility contrast

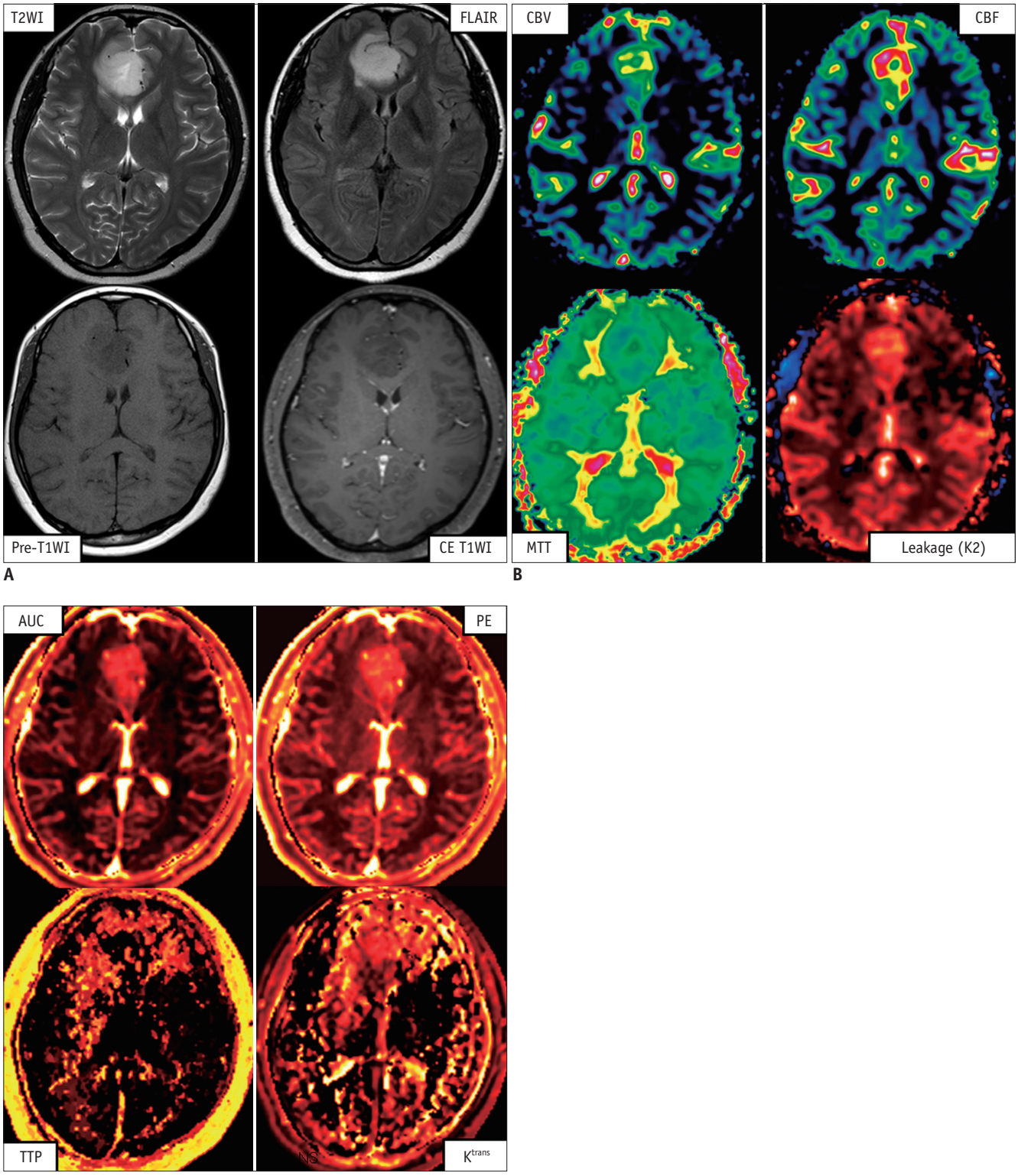

Fig. 4. Case of clinical application of perfusion MRI methods in patient with brain tumor.
MR images and parameter maps **(A)** calculated from data of both dynamic susceptibility-contrast MRI **(B)**, and dynamic contrast-enhanced MRI **(C)**, obtained from patient who has abaplastic astrocytoma (World Health Organization grade III) in frontal lobe in brain. Brain-blood barrier is intact (CE T1WI), but tumor vascularity is increased. AUC = area under curve, CBF = cerebral blood flow, CBV = cerebral blood volume, CE T1WI = T1-weighted image after injecting contrast agent, FLAIR = fluid attenuated inversion recovery image, MTT = mean transit time, PE = peak enhancement, Pre-T1WI = T1-weighted image before injecting contrast agent, TTP = time-to-peak, T2WI = T2-weighted image

Korean Journal of Radiology
KJR

calculated from DCE-MRI data obtained from the patient shown in Figure 4A. Increased AUC, peak enhancement, and K^{trans} values are shown in the frontal lesion, also indicating that tumor vascularity is increased.

ASL

Beyond its role in functional MRI, ASL is mainly applied in brain diseases (Fig. 5), such as neurodegenerative diseases to compare the quantitative CBF values among subject groups by voxel-based comparisons. CBF is altered in Alzheimer's disease and even in mild cognitive impairment (151-154). Due to its non-invasiveness, serial measurements with ASL could be useful in a number of applications, including the assessment of vascular reactivity (155). ASL was also applied to investigate treatment response in brain tumor (156, 157). Moreover, ASL was recently applied to evaluate heart, kidney, and muscle diseases. This method is especially attractive for patients with poor intravenous access, infants and children, and pregnant women. A further recent application for ASL is in functional connectivity (158, 159) and functional connectome studies (160), as a complementary method to blood-oxygen-level dependent functional MRI, but with the added benefit that it also provides information about a physiological parameter (i.e., CBF).

Summary

Dynamic susceptibility contrast-MRI is good for quick measurement of transit time, whole brain coverage, and fast scan time. DCE-MRI is good for measurements of blood volume and K^{trans} and for reducing imaging artifacts (Table 7). ASL is good for blood flow measurement, repeatable studies, and applications in children. Bolus methods with injections of a contrast agent provide better sensitivity with higher spatial resolution, but ASL methods provide the unique opportunity to provide CBF information without injections of the contrast agent and have better accuracy for quantification. The use of combined protocols that incorporate bolus methods of DSC and DCE with ASL

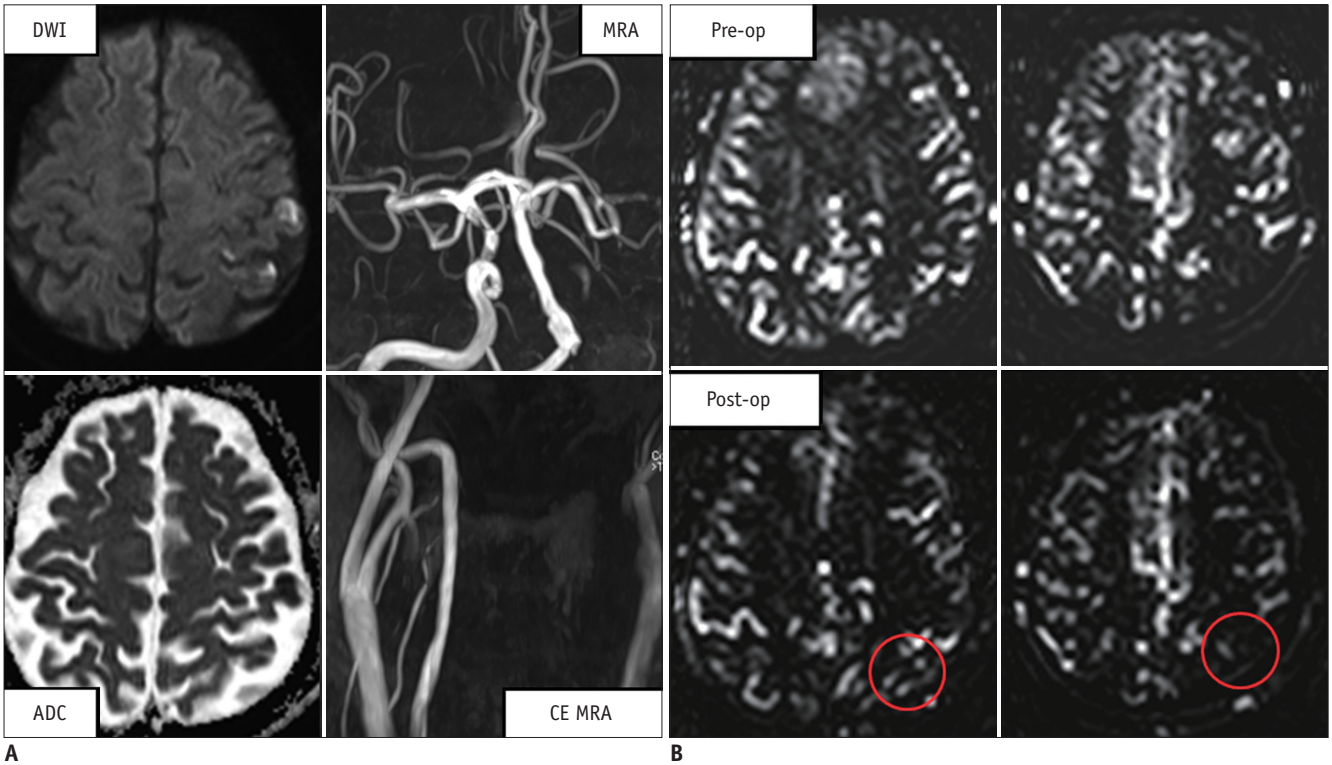

Fig. 5. Case of clinical application of arterial spin-labeling MRI in patient with brain infarction.
Magnetic resonance images **(A)**, and perfusion-weighted imaging **(B)**, before (Pre-op) and after (Post-op) bypass surgery, in 59-year-old male with border zone infarction. **A.** Image shows DWI obtained with b-value of 1000 s/mm^2, and corresponding ADC map, time-of-flight MRA, and CE MRA. High signal intensity on DWI at left side of brain indicates area with decreased diffusion, and MRA shows occlusion of middle cerebral artery. **B.** Image shows two slices of perfusion-weighted images before, and after bypass surgery. Slightly increased CBF is shown after bypass surgery. Only small amount of CBF is observed, because images were obtained immediately after bypass surgery. ADC = apparent diffusion coefficient, CBF = cerebral blood flow, CE MRA = magnetic resonance angiography with injecting contrast agent, DWI = diffusion-weighted imaging, MRA = magnetic resonance angiography with time-of-flight technique

Table 7. Advantages and Disadvantages of Perfusion Signals

	DSC	DCE	ASL	CT
Basis	T_2/T_2*	T_1	Spin tag	Density
Contrast agent	Gd-based	Gd-based	Blood label	Iodine
SNR	Very good	Good	Fair	Good
CBF	Fair	Poor	Very good	Good
CBV	Good	Very good	Poor	Very good
Transit	Very good (MTT)	Very good (K^{trans})	Fair	Very good
Coverage	Very good	Good	Good	Good
Scan time	Very good	Fair	Good	Very good
Repeatable	Good	Fair	Very good	Good
Child application	Good	Fair	Very good	Poor
Image artifact	Fair	Very good	Good	Good

Note.— Very good (+++), Good (++), Fair (+), Poor (-). ASL = arterial spin-labeling, CBF = cerebral blood flow, CBV = cerebral blood volume, CT = computed tomography, DCE = dynamic contrast-enhanced, DSC = dynamic susceptibility contrast, MTT = mean transit time, SNR = signal-to-noise ratio

techniques should have great impact on future clinical applications in patients.

Acknowledgments

We are appreciative of Dr. Eui Jong Kim at the Kyung Hee University Hospital in Seoul, Korea, for providing the clinical case data.

F.C. is grateful to the National Health and Medical Research Council (NHMRC) of Australia, the Australian Research Council (ARC), and the Victorian Government's Operational Infrastructure Support Grant, for their kind support.

REFERENCES

1. Rosen BR, Belliveau JW, Vevea JM, Brady TJ. Perfusion imaging with NMR contrast agents. *Magn Reson Med* 1990;14:249-265
2. Erlemann R, Reiser MF, Peters PE, Vasallo P, Nommensen B, Kusnierz-Glaz CR, et al. Musculoskeletal neoplasms: static and dynamic Gd-DTPA--enhanced MR imaging. *Radiology* 1989;171:767-773
3. Detre JA, Leigh JS, Williams DS, Koretsky AP. Perfusion imaging. *Magn Reson Med* 1992;23:37-45
4. Weisskoff RM, Zuo CS, Boxerman JL, Rosen BR. Microscopic susceptibility variation and transverse relaxation: theory and experiment. *Magn Reson Med* 1994;31:601-610
5. Simonsen CZ, Ostergaard L, Vestergaard-Poulsen P, Røhl L, Bjørnerud A, Gyldensted C. CBF and CBV measurements by USPIO bolus tracking: reproducibility and comparison with Gd-based values. *J Magn Reson Imaging* 1999;9:342-347
6. Stanisz GJ, Henkelman RM. Gd-DTPA relaxivity depends on macromolecular content. *Magn Reson Med* 2000;44:665-667
7. Pintaske J, Martirosian P, Graf H, Erb G, Lodemann KP, Claussen CD, et al. Relaxivity of Gadopentetate Dimeglumine (Magnevist), Gadobutrol (Gadovist), and Gadobenate Dimeglumine (MultiHance) in human blood plasma at 0.2, 1.5, and 3 Tesla. *Invest Radiol* 2006;41:213-221
8. Buckley DL, Kershaw LE, Stanisz GJ. Cellular-interstitial water exchange and its effect on the determination of contrast agent concentration in vivo: dynamic contrast-enhanced MRI of human internal obturator muscle. *Magn Reson Med* 2008;60:1011-1019
9. Wong EC. An introduction to ASL labeling techniques. *J Magn Reson Imaging* 2014;40:1-10
10. Williams DS, Detre JA, Leigh JS, Koretsky AP. Magnetic resonance imaging of perfusion using spin inversion of arterial water. *Proc Natl Acad Sci U S A* 1992;89:212-216
11. Alsop DC, Detre JA. Multisection cerebral blood flow MR imaging with continuous arterial spin labeling. *Radiology* 1998;208:410-416
12. Edelman RR, Siewert B, Darby DG, Thangaraj V, Nobre AC, Mesulam MM, et al. Qualitative mapping of cerebral blood flow and functional localization with echo-planar MR imaging and signal targeting with alternating radio frequency. *Radiology* 1994;192:513-520
13. Kwong KK, Chesler DA, Weisskoff RM, Donahue KM, Davis TL, Ostergaard L, et al. MR perfusion studies with T1-weighted echo planar imaging. *Magn Reson Med* 1995;34:878-887
14. Kim SG. Quantification of relative cerebral blood flow change by flow-sensitive alternating inversion recovery (FAIR) technique: application to functional mapping. *Magn Reson Med* 1995;34:293-301
15. Wong EC, Buxton RB, Frank LR. Implementation of quantitative perfusion imaging techniques for functional brain mapping using pulsed arterial spin labeling. *NMR Biomed* 1997;10:237-249
16. Pruessmann KP, Golay X, Stuber M, Scheidegger MB, Boesiger P. RF pulse concatenation for spatially selective inversion. *J Magn Reson* 2000;146:58-65
17. Jahng GH, Zhu XP, Matson GB, Weiner MW, Schuff N. Improved perfusion-weighted MRI by a novel double inversion with proximal labeling of both tagged and control

acquisitions. *Magn Reson Med* 2003;49:307-314
18. Jahng GH, Weiner MW, Schuff N. Improved arterial spin labeling method: applications for measurements of cerebral blood flow in human brain at high magnetic field MRI. *Med Phys* 2007;34:4519-4525
19. Wong EC, Cronin M, Wu WC, Inglis B, Frank LR, Liu TT. Velocity-selective arterial spin labeling. *Magn Reson Med* 2006;55:1334-1341
20. Kiselev VG. On the theoretical basis of perfusion measurements by dynamic susceptibility contrast MRI. *Magn Reson Med* 2001;46:1113-1122
21. Speck O, Chang L, DeSilva NM, Ernst T. Perfusion MRI of the human brain with dynamic susceptibility contrast: gradient-echo versus spin-echo techniques. *J Magn Reson Imaging* 2000;12:381-387
22. Zhu XP, Li KL, Kamaly-Asl ID, Checkley DR, Tessier JJ, Waterton JC, et al. Quantification of endothelial permeability, leakage space, and blood volume in brain tumors using combined T1 and T2* contrast-enhanced dynamic MR imaging. *J Magn Reson Imaging* 2000;11:575-585
23. Günther M, Bock M, Schad LR. Arterial spin labeling in combination with a look-locker sampling strategy: inflow turbo-sampling EPI-FAIR (ITS-FAIR). *Magn Reson Med* 2001;46:974-984
24. Brookes MJ, Morris PG, Gowland PA, Francis ST. Noninvasive measurement of arterial cerebral blood volume using Look-Locker EPI and arterial spin labeling. *Magn Reson Med* 2007;58:41-54
25. Francis ST, Bowtell R, Gowland PA. Modeling and optimization of Look-Locker spin labeling for measuring perfusion and transit time changes in activation studies taking into account arterial blood volume. *Magn Reson Med* 2008;59:316-325
26. Fernández-Seara MA, Wang Z, Wang J, Rao HY, Guenther M, Feinberg DA, et al. Continuous arterial spin labeling perfusion measurements using single shot 3D GRASE at 3 T. *Magn Reson Med* 2005;54:1241-1247
27. Günther M, Oshio K, Feinberg DA. Single-shot 3D imaging techniques improve arterial spin labeling perfusion measurements. *Magn Reson Med* 2005;54:491-498
28. Talagala SL, Ye FQ, Ledden PJ, Chesnick S. Whole-brain 3D perfusion MRI at 3.0 T using CASL with a separate labeling coil. *Magn Reson Med* 2004;52:131-140
29. Wong EC. New developments in arterial spin labeling pulse sequences. *NMR Biomed* 2013;26:887-891
30. Calamante F, Vonken EJ, van Osch MJ. Contrast agent concentration measurements affecting quantification of bolus-tracking perfusion MRI. *Magn Reson Med* 2007;58:544-553
31. Li KL, Buonaccorsi G, Thompson G, Cain JR, Watkins A, Russell D, et al. An improved coverage and spatial resolution--using dual injection dynamic contrast-enhanced (ICE-DICE) MRI: a novel dynamic contrast-enhanced technique for cerebral tumors. *Magn Reson Med* 2012;68:452-462
32. Alsop DC, Detre JA, Golay X, Günther M, Hendrikse J, Hernandez-Garcia L, et al. Recommended implementation of arterial spin-labeled perfusion MRI for clinical applications: a consensus of the ISMRM perfusion study group and the European consortium for ASL in dementia. *Magn Reson Med* 2014. doi: 10.1002/mrm.25197
33. Meier P, Zierler KL. On the theory of the indicator-dilution method for measurement of blood flow and volume. *J Appl Physiol* 1954;6:731-744
34. Ostergaard L, Weisskoff RM, Chesler DA, Gyldensted C, Rosen BR. High resolution measurement of cerebral blood flow using intravascular tracer bolus passages. Part I: Mathematical approach and statistical analysis. *Magn Reson Med* 1996;36:715-725
35. Thompson HK Jr, Starmer CF, Whalen RE, Mcintosh HD. Indicator transit time considered as a gamma variate. *Circ Res* 1964;14:502-515
36. Wong EC, Buxton RB, Frank LR. Quantitative imaging of perfusion using a single subtraction (QUIPSS and QUIPSS II). *Magn Reson Med* 1998;39:702-708
37. Luh WM, Wong EC, Bandettini PA, Hyde JS. QUIPSS II with thin-slice TI1 periodic saturation: a method for improving accuracy of quantitative perfusion imaging using pulsed arterial spin labeling. *Magn Reson Med* 1999;41:1246-1254
38. Detre JA, Alsop DC, Vives LR, Maccotta L, Teener JW, Raps EC. Noninvasive MRI evaluation of cerebral blood flow in cerebrovascular disease. *Neurology* 1998;50:633-641
39. Alsop DC, Detre JA. Reduced transit-time sensitivity in noninvasive magnetic resonance imaging of human cerebral blood flow. *J Cereb Blood Flow Metab* 1996;16:1236-1249
40. Paulson OB, Hertz MM, Bolwig TG, Lassen NA. Water filtration and diffusion across the blood brain barrier in man. *Acta Neurol Scand Suppl* 1977;64:492-493
41. Li KL, Zhu X, Hylton N, Jahng GH, Weiner MW, Schuff N. Four-phase single-capillary stepwise model for kinetics in arterial spin labeling MRI. *Magn Reson Med* 2005;53:511-518
42. Starmer CF, Clark DO. Computer computations of cardiac output using the gamma function. *J Appl Physiol* 1970;28:219-220
43. Weisskoff RM, Chesler D, Boxerman JL, Rosen BR. Pitfalls in MR measurement of tissue blood flow with intravascular tracers: which mean transit time? *Magn Reson Med* 1993;29:553-558
44. Calamante F, Thomas DL, Pell GS, Wiersma J, Turner R. Measuring cerebral blood flow using magnetic resonance imaging techniques. *J Cereb Blood Flow Metab* 1999;19:701-735
45. Calamante F, Gadian DG, Connelly A. Quantification of perfusion using bolus tracking magnetic resonance imaging in stroke: assumptions, limitations, and potential implications for clinical use. *Stroke* 2002;33:1146-1151
46. Calamante F. Arterial input function in perfusion MRI: a comprehensive review. *Prog Nucl Magn Reson Spectrosc* 2013;74:1-32
47. Rosen BR, Belliveau JW, Buchbinder BR, McKinstry RC,

Porkka LM, Kennedy DN, et al. Contrast agents and cerebral hemodynamics. *Magn Reson Med* 1991;19:285-292
48. Benner T, Heiland S, Erb G, Forsting M, Sartor K. Accuracy of gamma-variate fits to concentration-time curves from dynamic susceptibility-contrast enhanced MRI: influence of time resolution, maximal signal drop and signal-to-noise. *Magn Reson Imaging* 1997;15:307-317
49. Wu Y, An H, Krim H, Lin W. An independent component analysis approach for minimizing effects of recirculation in dynamic susceptibility contrast magnetic resonance imaging. *J Cereb Blood Flow Metab* 2007;27:632-645
50. Calamante F. Bolus dispersion issues related to the quantification of perfusion MRI data. *J Magn Reson Imaging* 2005;22:718-722
51. Wirestam R, Andersson L, Ostergaard L, Bolling M, Aunola JP, Lindgren A, et al. Assessment of regional cerebral blood flow by dynamic susceptibility contrast MRI using different deconvolution techniques. *Magn Reson Med* 2000;43:691-700
52. Calamante F, Gadian DG, Connelly A. Delay and dispersion effects in dynamic susceptibility contrast MRI: simulations using singular value decomposition. *Magn Reson Med* 2000;44:466-473
53. Wu O, Østergaard L, Weisskoff RM, Benner T, Rosen BR, Sorensen AG. Tracer arrival timing-insensitive technique for estimating flow in MR perfusion-weighted imaging using singular value decomposition with a block-circulant deconvolution matrix. *Magn Reson Med* 2003;50:164-174
54. Gall P, Emerich P, Kjølby BF, Kellner E, Mader I, Kiselev VG. On the design of filters for Fourier and oSVD-based deconvolution in bolus tracking perfusion MRI. *MAGMA* 2010;23:187-195
55. Calamante F, Gadian DG, Connelly A. Quantification of bolus-tracking MRI: improved characterization of the tissue residue function using Tikhonov regularization. *Magn Reson Med* 2003;50:1237-1247
56. Zanderigo F, Bertoldo A, Pillonetto G, Cobelli Ast C. Nonlinear stochastic regularization to characterize tissue residue function in bolus-tracking MRI: assessment and comparison with SVD, block-circulant SVD, and Tikhonov. *IEEE Trans Biomed Eng* 2009;56:1287-1297
57. Vonken EJ, van Osch MJ, Bakker CJ, Viergever MA. Measurement of cerebral perfusion with dual-echo multi-slice quantitative dynamic susceptibility contrast MRI. *J Magn Reson Imaging* 1999;10:109-117
58. Willats L, Connelly A, Calamante F. Minimising the effects of bolus dispersion in bolus-tracking MRI. *NMR Biomed* 2008;21:1126-1137
59. Willats L, Connelly A, Calamante F. Improved deconvolution of perfusion MRI data in the presence of bolus delay and dispersion. *Magn Reson Med* 2006;56:146-156
60. Grüner R, Taxt T. Iterative blind deconvolution in magnetic resonance brain perfusion imaging. *Magn Reson Med* 2006;55:805-815
61. Mehndiratta A, Calamante F, Macintosh BJ, Crane DE, Payne SJ, Chappell MA. Modeling and correction of bolus dispersion effects in dynamic susceptibility contrast MRI. *Magn Reson Med* 2014. doi: 10.1002/mrm.25077
62. Mouridsen K, Friston K, Hjort N, Gyldensted L, Østergaard L, Kiebel S. Bayesian estimation of cerebral perfusion using a physiological model of microvasculature. *Neuroimage* 2006;33:570-579
63. Kao YH, Guo WY, Wu YT, Liu KC, Chai WY, Lin CY, et al. Hemodynamic segmentation of MR brain perfusion images using independent component analysis, thresholding, and Bayesian estimation. *Magn Reson Med* 2003;49:885-894
64. Kidwell CS, Saver JL, Mattiello J, Starkman S, Vinuela F, Duckwiler G, et al. Thrombolytic reversal of acute human cerebral ischemic injury shown by diffusion/perfusion magnetic resonance imaging. *Ann Neurol* 2000;47:462-469
65. Calamante F, Christensen S, Desmond PM, Ostergaard L, Davis SM, Connelly A. The physiological significance of the time-to-maximum (Tmax) parameter in perfusion MRI. *Stroke* 2010;41:1169-1174
66. Tofts PS, Brix G, Buckley DL, Evelhoch JL, Henderson E, Knopp MV, et al. Estimating kinetic parameters from dynamic contrast-enhanced T(1)-weighted MRI of a diffusable tracer: standardized quantities and symbols. *J Magn Reson Imaging* 1999;10:223-232
67. Jackson A, Li KL, Zhu X. Semi-quantitative parameter analysis of DCE-MRI revisited: monte-carlo simulation, clinical comparisons, and clinical validation of measurement errors in patients with type 2 neurofibromatosis. *PLoS One* 2014;9:e90300
68. Tofts PS. Modeling tracer kinetics in dynamic Gd-DTPA MR imaging. *J Magn Reson Imaging* 1997;7:91-101
69. St Lawrence KS, Lee TY. An adiabatic approximation to the tissue homogeneity model for water exchange in the brain: II. Experimental validation. *J Cereb Blood Flow Metab* 1998;18:1378-1385
70. Brix G, Bahner ML, Hoffmann U, Horvath A, Schreiber W. Regional blood flow, capillary permeability, and compartmental volumes: measurement with dynamic CT--initial experience. *Radiology* 1999;210:269-276
71. Larsson HB, Courivaud F, Rostrup E, Hansen AE. Measurement of brain perfusion, blood volume, and blood-brain barrier permeability, using dynamic contrast-enhanced T(1)-weighted MRI at 3 tesla. *Magn Reson Med* 2009;62:1270-1281
72. Kety SS, Schmidt CF. The nitrous oxide method for the quantitative determination of cerebral blood flow in man: theory, procedure and normal values. *J Clin Invest* 1948;27:476-483
73. Buxton RB, Frank LR, Wong EC, Siewert B, Warach S, Edelman RR. A general kinetic model for quantitative perfusion imaging with arterial spin labeling. *Magn Reson Med* 1998;40:383-396
74. Willats L, Calamante F. The 39 steps: evading error and deciphering the secrets for accurate dynamic susceptibility contrast MRI. *NMR Biomed* 2013;26:913-931

75. Calamante F, Connelly A, van Osch MJ. Nonlinear DeltaR*2 effects in perfusion quantification using bolus-tracking MRI. *Magn Reson Med* 2009;61:486-492
76. Calamante F, Willats L, Gadian DG, Connelly A. Bolus delay and dispersion in perfusion MRI: implications for tissue predictor models in stroke. *Magn Reson Med* 2006;55:1180-1185
77. Calamante F, Yim PJ, Cebral JR. Estimation of bolus dispersion effects in perfusion MRI using image-based computational fluid dynamics. *Neuroimage* 2003;19(2 Pt 1):341-353
78. Calamante F, Mørup M, Hansen LK. Defining a local arterial input function for perfusion MRI using independent component analysis. *Magn Reson Med* 2004;52:789-797
79. Willats L, Christensen S, Ma HK, Donnan GA, Connelly A, Calamante F. Validating a local Arterial Input Function method for improved perfusion quantification in stroke. *J Cereb Blood Flow Metab* 2011;31:2189-2198
80. Lorenz C, Benner T, Chen PJ, Lopez CJ, Ay H, Zhu MW, et al. Automated perfusion-weighted MRI using localized arterial input functions. *J Magn Reson Imaging* 2006;24:1133-1139
81. van Osch MJ, Vonken EJ, Viergever MA, van der Grond J, Bakker CJ. Measuring the arterial input function with gradient echo sequences. *Magn Reson Med* 2003;49:1067-1076
82. Bleeker EJ, van Buchem MA, van Osch MJ. Optimal location for arterial input function measurements near the middle cerebral artery in first-pass perfusion MRI. *J Cereb Blood Flow Metab* 2009;29:840-852
83. Bleeker EJ, van Osch MJ, Connelly A, van Buchem MA, Webb AG, Calamante F. New criterion to aid manual and automatic selection of the arterial input function in dynamic susceptibility contrast MRI. *Magn Reson Med* 2011;65:448-456
84. Bjornerud A, Sorensen AG, Mouridsen K, Emblem KE. T1- and T2*-dominant extravasation correction in DSC-MRI: part I--theoretical considerations and implications for assessment of tumor hemodynamic properties. *J Cereb Blood Flow Metab* 2011;31:2041-2053
85. Boxerman JL, Hamberg LM, Rosen BR, Weisskoff RM. MR contrast due to intravascular magnetic susceptibility perturbations. *Magn Reson Med* 1995;34:555-566
86. Shin W, Horowitz S, Ragin A, Chen Y, Walker M, Carroll TJ. Quantitative cerebral perfusion using dynamic susceptibility contrast MRI: evaluation of reproducibility and age- and gender-dependence with fully automatic image postprocessing algorithm. *Magn Reson Med* 2007;58:1232-1241
87. Zaharchuk G, Straka M, Marks MP, Albers GW, Moseley ME, Bammer R. Combined arterial spin label and dynamic susceptibility contrast measurement of cerebral blood flow. *Magn Reson Med* 2010;63:1548-1556
88. Bonekamp D, Degaonkar M, Barker PB. Quantitative cerebral blood flow in dynamic susceptibility contrast MRI using total cerebral flow from phase contrast magnetic resonance angiography. *Magn Reson Med* 2011;66:57-66
89. Parker GJ, Baustert I, Tanner SF, Leach MO. Improving image quality and T(1) measurements using saturation recovery turboFLASH with an approximate K-space normalisation filter. *Magn Reson Imaging* 2000;18:157-167
90. Buckley DL. Uncertainty in the analysis of tracer kinetics using dynamic contrast-enhanced T1-weighted MRI. *Magn Reson Med* 2002;47:601-606
91. Landis CS, Li X, Telang FW, Coderre JA, Micca PL, Rooney WD, et al. Determination of the MRI contrast agent concentration time course in vivo following bolus injection: effect of equilibrium transcytolemmal water exchange. *Magn Reson Med* 2000;44:563-574
92. Silver MS, Joseph RI, Hoult DI. Selective spin inversion in nuclear magnetic resonance and coherent optics through an exact solution of the Bloch-Riccati equation. *Phys Rev A* 1985;31:2753-2755
93. Ordidge RJ, Wylezinska M, Hugg JW, Butterworth E, Franconi F. Frequency offset corrected inversion (FOCI) pulses for use in localized spectroscopy. *Magn Reson Med* 1996;36:562-566
94. Warnking JM, Pike GB. Bandwidth-modulated adiabatic RF pulses for uniform selective saturation and inversion. *Magn Reson Med* 2004;52:1190-1199
95. Dixon WT, Sardashti M, Castillo M, Stomp GP. Multiple inversion recovery reduces static tissue signal in angiograms. *Magn Reson Med* 1991;18:257-268
96. Ye FQ, Frank JA, Weinberger DR, McLaughlin AC. Noise reduction in 3D perfusion imaging by attenuating the static signal in arterial spin tagging (ASSIST). *Magn Reson Med* 2000;44:92-100
97. Alsop DC. Arterial spin labeling: its time is now. *MAGMA* 2012;25:75-77
98. Jahng GH, Stables L, Ebel A, Matson GB, Meyerhoff DJ, Weiner MW, et al. Sensitive and fast T1 mapping based on two inversion recovery images and a reference image. *Med Phys* 2005;32:1524-1528
99. Yang Y, Engelien W, Xu S, Gu H, Silbersweig DA, Stern E. Transit time, trailing time, and cerebral blood flow during brain activation: measurement using multislice, pulsed spin-labeling perfusion imaging. *Magn Reson Med* 2000;44:680-685
100. Gonzalez-At JB, Alsop DC, Detre JA. Cerebral perfusion and arterial transit time changes during task activation determined with continuous arterial spin labeling. *Magn Reson Med* 2000;43:739-746
101. Chen Y, Wang DJ, Detre JA. Comparison of arterial transit times estimated using arterial spin labeling. *MAGMA* 2012;25:135-144
102. Asllani I, Borogovac A, Brown TR. Regression algorithm correcting for partial volume effects in arterial spin labeling MRI. *Magn Reson Med* 2008;60:1362-1371
103. Liang X, Connelly A, Calamante F. Improved partial volume correction for single inversion time arterial spin labeling data. *Magn Reson Med* 2013;69:531-537
104. Chappell MA, Groves AR, MacIntosh BJ, Donahue MJ, Jezzard

P, Woolrich MW. Partial volume correction of multiple inversion time arterial spin labeling MRI data. *Magn Reson Med* 2011;65:1173-1183
105. Kiselev VG. Transverse relaxation effect of MRI contrast agents: a crucial issue for quantitative measurements of cerebral perfusion. *J Magn Reson Imaging* 2005;22:693-696
106. Bleeker EJ, van Buchem MA, Webb AG, van Osch MJ. Phase-based arterial input function measurements for dynamic susceptibility contrast MRI. *Magn Reson Med* 2010;64:358-368
107. Straka M, Albers GW, Bammer R. Real-time diffusion-perfusion mismatch analysis in acute stroke. *J Magn Reson Imaging* 2010;32:1024-1037
108. Kim J, Leira EC, Callison RC, Ludwig B, Moritani T, Magnotta VA, et al. Toward fully automated processing of dynamic susceptibility contrast perfusion MRI for acute ischemic cerebral stroke. *Comput Methods Programs Biomed* 2010;98:204-213
109. Bjørnerud A, Emblem KE. A fully automated method for quantitative cerebral hemodynamic analysis using DSC-MRI. *J Cereb Blood Flow Metab* 2010;30:1066-1078
110. Dai W, Garcia D, de Bazelaire C, Alsop DC. Continuous flow-driven inversion for arterial spin labeling using pulsed radio frequency and gradient fields. *Magn Reson Med* 2008;60:1488-1497
111. Garcia DM, Duhamel G, Alsop DC. Efficiency of inversion pulses for background suppressed arterial spin labeling. *Magn Reson Med* 2005;54:366-372
112. Zaharchuk G, Ledden PJ, Kwong KK, Reese TG, Rosen BR, Wald LL. Multislice perfusion and perfusion territory imaging in humans with separate label and image coils. *Magn Reson Med* 1999;41:1093-1098
113. Paiva FF, Tannús A, Talagala SL, Silva AC. Arterial spin labeling of cerebral perfusion territories using a separate labeling coil. *J Magn Reson Imaging* 2008;27:970-977
114. Helle M, Rüfer S, Alfke K, Jansen O, Norris DG. Perfusion territory imaging of intracranial branching arteries - optimization of continuous artery-selective spin labeling (CASSL). *NMR Biomed* 2011;24:404-412
115. Davies NP, Jezzard P. Selective arterial spin labeling (SASL): perfusion territory mapping of selected feeding arteries tagged using two-dimensional radiofrequency pulses. *Magn Reson Med* 2003;49:1133-1142
116. Hendrikse J, van der Grond J, Lu H, van Zijl PC, Golay X. Flow territory mapping of the cerebral arteries with regional perfusion MRI. *Stroke* 2004;35:882-887
117. Zimine I, Petersen ET, Golay X. Dual vessel arterial spin labeling scheme for regional perfusion imaging. *Magn Reson Med* 2006;56:1140-1144
118. Günther M. Efficient visualization of vascular territories in the human brain by cycled arterial spin labeling MRI. *Magn Reson Med* 2006;56:671-675
119. Wong EC. Vessel-encoded arterial spin-labeling using pseudocontinuous tagging. *Magn Reson Med* 2007;58:1086-1091
120. Chappell MA, Okell TW, Jezzard P, Woolrich MW. A general framework for the analysis of vessel encoded arterial spin labeling for vascular territory mapping. *Magn Reson Med* 2010;64:1529-1539
121. Helle M, Norris DG, Rüfer S, Alfke K, Jansen O, van Osch MJ. Superselective pseudocontinuous arterial spin labeling. *Magn Reson Med* 2010;64:777-786
122. Hartkamp NS, Petersen ET, De Vis JB, Bokkers RP, Hendrikse J. Mapping of cerebral perfusion territories using territorial arterial spin labeling: techniques and clinical application. *NMR Biomed* 2013;26:901-912
123. Larkman DJ, Hajnal JV, Herlihy AH, Coutts GA, Young IR, Ehnholm G. Use of multicoil arrays for separation of signal from multiple slices simultaneously excited. *J Magn Reson Imaging* 2001;13:313-317
124. Feinberg DA, Beckett A, Chen L. Arterial spin labeling with simultaneous multi-slice echo planar imaging. *Magn Reson Med* 2013;70:1500-1506
125. Kim T, Shin W, Zhao T, Beall EB, Lowe MJ, Bae KT. Whole brain perfusion measurements using arterial spin labeling with multiband acquisition. *Magn Reson Med* 2013;70:1653-1661
126. Dixon WT, Du LN, Faul DD, Gado M, Rossnick S. Projection angiograms of blood labeled by adiabatic fast passage. *Magn Reson Med* 1986;3:454-462
127. Robson PM, Dai W, Shankaranarayanan A, Rofsky NM, Alsop DC. Time-resolved vessel-selective digital subtraction MR angiography of the cerebral vasculature with arterial spin labeling. *Radiology* 2010;257:507-515
128. Petersen ET, Lim T, Golay X. Model-free arterial spin labeling quantification approach for perfusion MRI. *Magn Reson Med* 2006;55:219-232
129. Silva AC, Williams DS, Koretsky AP. Evidence for the exchange of arterial spin-labeled water with tissue water in rat brain from diffusion-sensitized measurements of perfusion. *Magn Reson Med* 1997;38:232-237
130. Saver JL. Time is brain--quantified. *Stroke* 2006;37:263-266
131. Covarrubias DJ, Rosen BR, Lev MH. Dynamic magnetic resonance perfusion imaging of brain tumors. *Oncologist* 2004;9:528-537
132. Waldman AD, Jackson A, Price SJ, Clark CA, Booth TC, Auer DP, et al. Quantitative imaging biomarkers in neuro-oncology. *Nat Rev Clin Oncol* 2009;6:445-454
133. Sourbron S, Ingrisch M, Siefert A, Reiser M, Herrmann K. Quantification of cerebral blood flow, cerebral blood volume, and blood-brain-barrier leakage with DCE-MRI. *Magn Reson Med* 2009;62:205-217
134. Moody AR, Martel A, Kenton A, Allder S, Horsfield MA, Delay G, et al. Contrast-reduced imaging of tissue concentration and arterial level (CRITICAL) for assessment of cerebral hemodynamics in acute stroke by magnetic resonance. *Invest Radiol* 2000;35:401-411
135. Martel AL, Allder SJ, Delay GS, Morgan PS, Moody AA. Perfusion MRI of infarcted and noninfarcted brain tissue in stroke: a comparison of conventional hemodynamic imaging

and factor analysis of dynamic studies. *Invest Radiol* 2001;36:378-385
136. Singh A, Haris M, Rathore D, Purwar A, Sarma M, Bayu G, et al. Quantification of physiological and hemodynamic indices using T(1) dynamic contrast-enhanced MRI in intracranial mass lesions. *J Magn Reson Imaging* 2007;26:871-880
137. Larsson HB, Hansen AE, Berg HK, Rostrup E, Haraldseth O. Dynamic contrast-enhanced quantitative perfusion measurement of the brain using T1-weighted MRI at 3T. *J Magn Reson Imaging* 2008;27:754-762
138. Leigh R, Jen SS, Varma DD, Hillis AE, Barker PB. Arrival time correction for dynamic susceptibility contrast MR permeability imaging in stroke patients. *PLoS One* 2012;7:e52656
139. Law M, Yang S, Babb JS, Knopp EA, Golfinos JG, Zagzag D, et al. Comparison of cerebral blood volume and vascular permeability from dynamic susceptibility contrast-enhanced perfusion MR imaging with glioma grade. *AJNR Am J Neuroradiol* 2004;25:746-755
140. Kim EJ, Kim DH, Lee SH, Huh YM, Song HT, Suh JS. Simultaneous acquisition of perfusion and permeability from corrected relaxation rates with dynamic susceptibility contrast dual gradient echo. *Magn Reson Imaging* 2004;22:307-314
141. Provenzale JM, Wang GR, Brenner T, Petrella JR, Sorensen AG. Comparison of permeability in high-grade and low-grade brain tumors using dynamic susceptibility contrast MR imaging. *AJR Am J Roentgenol* 2002;178:711-716
142. Larsson HB, Stubgaard M, Frederiksen JL, Jensen M, Henriksen O, Paulson OB. Quantitation of blood-brain barrier defect by magnetic resonance imaging and gadolinium-DTPA in patients with multiple sclerosis and brain tumors. *Magn Reson Med* 1990;16:117-131
143. Tofts PS, Kermode AG. Measurement of the blood-brain barrier permeability and leakage space using dynamic MR imaging. 1. Fundamental concepts. *Magn Reson Med* 1991;17:357-367
144. Materne R, Smith AM, Peeters F, Dehoux JP, Keyeux A, Horsmans Y, et al. Assessment of hepatic perfusion parameters with dynamic MRI. *Magn Reson Med* 2002;47:135-142
145. Choyke PL, Dwyer AJ, Knopp MV. Functional tumor imaging with dynamic contrast-enhanced magnetic resonance imaging. *J Magn Reson Imaging* 2003;17:509-520
146. Jerosch-Herold M, Seethamraju RT, Swingen CM, Wilke NM, Stillman AE. Analysis of myocardial perfusion MRI. *J Magn Reson Imaging* 2004;19:758-770
147. Brix G, Kiessling F, Lucht R, Darai S, Wasser K, Delorme S, et al. Microcirculation and microvasculature in breast tumors: pharmacokinetic analysis of dynamic MR image series. *Magn Reson Med* 2004;52:420-429
148. Dujardin M, Sourbron S, Luypaert R, Verbeelen D, Stadnik T. Quantification of renal perfusion and function on a voxel-by-voxel basis: a feasibility study. *Magn Reson Med* 2005;54:841-849
149. Pandharipande PV, Krinsky GA, Rusinek H, Lee VS. Perfusion imaging of the liver: current challenges and future goals. *Radiology* 2005;234:661-673
150. Kershaw LE, Hutchinson CE, Buckley DL. Benign prostatic hyperplasia: evaluation of T1, T2, and microvascular characteristics with T1-weighted dynamic contrast-enhanced MRI. *J Magn Reson Imaging* 2009;29:641-648
151. Kim SM, Kim MJ, Rhee HY, Ryu CW, Kim EJ, Petersen ET, et al. Regional cerebral perfusion in patients with Alzheimer's disease and mild cognitive impairment: effect of APOE epsilon4 allele. *Neuroradiology* 2013;55:25-34
152. Du AT, Jahng GH, Hayasaka S, Kramer JH, Rosen HJ, Gorno-Tempini ML, et al. Hypoperfusion in frontotemporal dementia and Alzheimer disease by arterial spin labeling MRI. *Neurology* 2006;67:1215-1220
153. Hayasaka S, Du AT, Duarte A, Kornak J, Jahng GH, Weiner MW, et al. A non-parametric approach for co-analysis of multi-modal brain imaging data: application to Alzheimer's disease. *Neuroimage* 2006;30:768-779
154. Johnson NA, Jahng GH, Weiner MW, Miller BL, Chui HC, Jagust WJ, et al. Pattern of cerebral hypoperfusion in Alzheimer disease and mild cognitive impairment measured with arterial spin-labeling MR imaging: initial experience. *Radiology* 2005;234:851-859
155. Bokkers RP, van Osch MJ, Klijn CJ, Kappelle LJ, Hendrikse J. Cerebrovascular reactivity within perfusion territories in patients with an internal carotid artery occlusion. *J Neurol Neurosurg Psychiatry* 2011;82:1011-1016
156. Song YS, Choi SH, Park CK, Yi KS, Lee WJ, Yun TJ, et al. True progression versus pseudoprogression in the treatment of glioblastomas: a comparison study of normalized cerebral blood volume and apparent diffusion coefficient by histogram analysis. *Korean J Radiol* 2013;14:662-672
157. Choi YJ, Kim HS, Jahng GH, Kim SJ, Suh DC. Pseudoprogression in patients with glioblastoma: added value of arterial spin labeling to dynamic susceptibility contrast perfusion MR imaging. *Acta Radiol* 2013;54:448-454
158. Haller S, Rodriguez C, Moser D, Toma S, Hofmeister J, Sinanaj I, et al. Acute caffeine administration impact on working memory-related brain activation and functional connectivity in the elderly: a BOLD and perfusion MRI study. *Neuroscience* 2013;250:364-371
159. Liang X, Tournier JD, Masterton R, Connelly A, Calamante F. A k-space sharing 3D GRASE pseudocontinuous ASL method for whole-brain resting-state functional connectivity. *Int J Imaging Syst Technol* 2012;22:37-43
160. Liang X, Connelly A, Calamante F. Graph analysis of resting-state ASL perfusion MRI data: nonlinear correlations among CBF and network metrics. *Neuroimage* 2014;87:265-275